© 2018. This manuscript version is made available under the CC-BY-NC-ND 4.0 license http://creativecommons.org/licenses/by-nc-nd/4.0/

Experimental and Computational Fluid Dynamics study of separation gap effect on gas explosion mitigation for methane storage tanks

Jingde Li[1, a], Hong Hao[2, b], Yanchao Shi[3,c], Qin Fang[4,d], Zhan Li[4,e], Li Chen[4, f]

[1]Center for Infrastructure monitoring and protection, School of Civil and Mechanical Engineering, Curtin University, Kent St, Bentley WA 6102, Australia

[2]Tianjin University and Curtin University Joint Research Centre of Structural Monitoring and Protection, School of Civil and Mechanical Engineering, Curtin University, Kent St, Bentley WA 6102, Australia and School of Civil Engineering, Guangzhou University, China

[3]School of Civil Engineering, Tianjin University, Tianjin 300072, China

[4]PLA University of Science and Technology, No. 88 Hou Biao Ying Road, Nanjing 210007, Jiangsu, People's Republic of China

[a]jingde.li@curtin.edu.au, [b]hong.hao@curtin.edu.au, [c]yanchaoshi@tju.edu.cn, [d]fangqinjs@139.com, [e]lz.9008@163.com, [f]chenli1360@qq.com

Abstract

This paper presented both experimental and numerical assessments of separation gap effect on vented explosion pressure in and around the area of a tank group. A series of vented gas explosion layouts with different separation gaps between tanks were experimentally investigated. In order to qualitatively determine the relationship between the separation gap distance and explosion pressure, intensive computational Fluid Dynamics (CFD) simulations, verified with testing data, were conducted. Good agreement between CFD simulation results and experimental data was achieved. By using CFD simulation, more gas explosion cases were included to consider different gas cloud coverage scenarios. Separation gap effects on internal and external pressures at various locations were investigated.

© 2018. This manuscript version is made available under the CC-BY-NC-ND 4.0 license http://creativecommons.org/licenses/by-nc-nd/4.0/

Keywords: separation gap; safety gap; external pressure; vented gas explosion; CFD; FLACS

1. Introduction

Physical layout of element spacing is one of the primary issues of Liquefied natural gas (LNG) project modeling (Taylor, 2007). The internationally recognized standard NFPA-59A (NFPA-59A, 2016) and European standard EN-1473 (EN-1473, 2016) are often used to ensure code compliance of the plant spacing issue. The separation spacing requirements for tanks are specified based on the empirical calculations by considering the volume of the tanks and the allowable heat flux values in NFPA-59A. Whereas the separation distance between two containers is determined by a detailed hazard assessment in EN-1473 (Raj and Lemoff, 2009).

For large tanks with storage capacity over 265 m^3, NFPA-59A requires the safe spacing between tanks no less than $1/4^{th}$ of the sum of the diameters of adjacent tanks, while only 1m or 1.5m minimum distance is specified for tanks smaller than 265 m^3 (NFPA-59A, 2016). In terms of the EN-1473, the minimum separation distance should be no less than half of the secondary tank's diameter. Nevertheless, there are no fine subdivisions of separation distances according to the relationship between separation distance and tank diameter in these codes.

In order to better understand the impact of separation distance/gap on tank layout design, engineers and researchers had conducted more studies based on the industrial standards. For instance, a Computational Fluid Dynamics (CFD) study was carried out by Santos and Landesmann (Santos and Landesmann, 2014) to investigate the separation gap effect on the safety of fuel storage tank farms. A specific minimum safety distance recommendation was proposed. However, the analysis was conducted on storage tanks subjected to fire conditions, the explosion pressure was not taken into account. Zhang et al. (Zhang et al., 2017) had conducted a more detailed safety analysis on tank farm layout optimizations. An integrated

© 2018. This manuscript version is made available under the CC-BY-NC-ND 4.0 license http://creativecommons.org/licenses/by-nc-nd/4.0/

probabilistic framework along with some relevant procedures were developed to optimize the space collocation on the basis of different acceptable thermal radiation. Other literatures focusing on optimizing cost by means of different safety distances/gaps were also reported (Diaz-Ovalle et al., 2010; Jung et al., 2011; Patsiatzis et al., 2004). In the study of optimization of facility layout by Jung et al. (Jung et al., 2011), the gas explosion scenarios were modelled by conducting CFD simulation, the flame acceleration simulator (FLACS) was only used as an accessional calibrator to assess the financially optimized layout. The relationship between safety distance and explosion overpressure was not discussed.

Overall, the models in the industry standards and the majority of current studies on safety distance determination are based on the flammability of the contents, thermal radiation data and financial risk management. Little attention has been paid on the consequence of gas explosion, such as the explosion overpressure and its effect on adjacent structures.

In this study, the separation distance effect on gas explosion overpressure was thoroughly investigated. Experiments were conducted on a group of tanks. A series of tank layouts with different separation gaps were designed in the testing. The gas clouds were ignited inside a vented tank. CFD simulation was conducted to qualitatively study the relationship between the separation gap distance and explosion overpressure. Two different gas cloud coverage scenarios were taken into account. The internal and external pressures subjected to different separation gaps were calculated and discussed.

2. Experimental tank group explosion tests

In the tank group explosion tests, the cylindrical tanks designed according to American Petroleum Institute Standard (API-650, 2007) were used. All tanks are 1.0m in height and 1.5m in diameter. Same as the tanks used in previous study (Li et al., 2017), the tested tanks are

© 2018. This manuscript version is made available under the CC-BY-NC-ND 4.0 license http://creativecommons.org/licenses/by-nc-nd/4.0/

made of steel Q345B with tensile strength 470 MPa and yield strength 345 MPa. The welding between the tank roof and wall has yield strength 450 MPa and tensile strength 530 MPa.

2.1 Experimental details

As seen in Fig. 1, a tank with two venting panels was surrounded by 7 enclosed tanks and 1 upright truss fixed on the ground. 6 piezo-resistive sensors (CYG 1409, Kunshan Shuangqiao Sensors, China), with a pressure measuring range of 0 to 150 kPa, were used in the testing. Pressure sensors on the tank wall were mounted by using hex nuts, and rubber washers were used to ensure the impermeability of equipment. Signals from pressure sensors were logged on a 16-Bit A/D converter sampling at 100 kHz. Two sensors named as Sensor 1- (West-direction) and Sensor 1+ (East-direction) were mounted on the internal wall of the center tank to measure internal pressure, while another two sensors (i.e. Sensor 2 and Sensor 3) were fixed onto the neighboring tanks to measure external pressures. Fig. 2 illustrates the sensor's detail and location on the center tank. Extra two sensors (i.e. Sensor 4 and Sensor 5) were mounted on the truss to monitor the external pressure in the venting direction, and fire-resistant coating was applied for all sensors, as seen in Fig. 3. Ambient temperature was approximately 26°C in the field during the tests. Wind speed was 2.8 m/s.

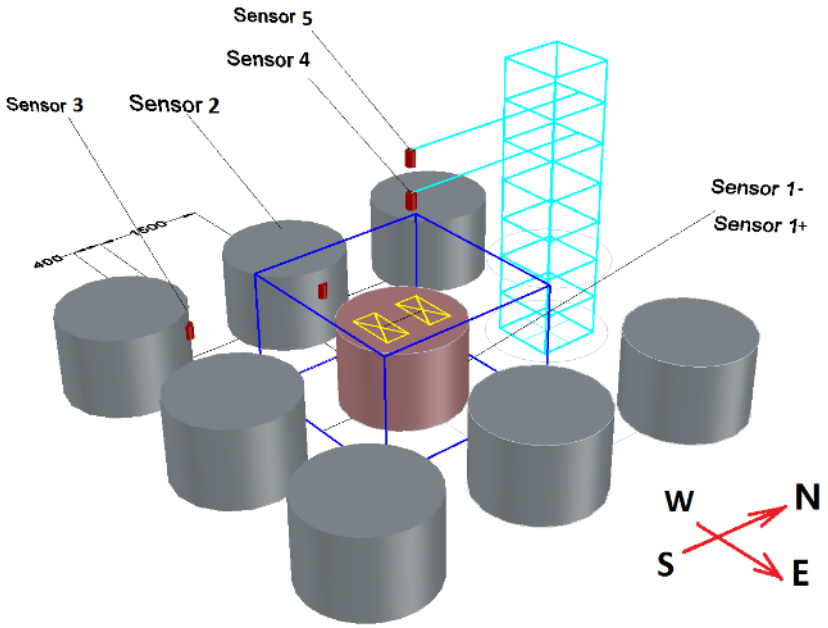

© 2018. This manuscript version is made available under the CC-BY-NC-ND 4.0 license http://creativecommons.org/licenses/by-nc-nd/4.0/

Fig. 1 Tank group testing setup in 3D view

(a) piezo-resistive sensor **(b) sensor mounted on the center tank wall**

Fig. 2 Piezo-resistive sensor detail and location on the tank

(a) Two sensors mounted on the truss **(b) fire-resistant coating on a sensor**

Fig. 3 Sensors above the tank group and fire protection for sensors

The tank located in the center had two symmetric venting areas with dimensions of 305×610 mm^2, as seen in Fig. 4 (a). The vents were kept as open during the gas mixing and explosion testing. A 0.015mm polyethylene film was used to confine an enclosed region with dimensions of 2300×2300×1500 mm^3, the center tank was located inside the confined region, as seen in Fig. 4 (b). Four vales with cross-section size of 1.9 cm diameter were mounted on the center tank wall. Two of the valves were connected to air inlet and gas inlet, while another two valves on other side were connected to air outlet and gas outlet.

© 2018. This manuscript version is made available under the CC-BY-NC-ND 4.0 license http://creativecommons.org/licenses/by-nc-nd/4.0/

105
106 **(a) Venting areas on the tank top**

107
108 **(b) Methane-air mixing inlet & outlet valves**

109 **Fig. 4 Center tank with two venting areas and four valves in the tank group explosion testing**

110

© 2018. This manuscript version is made available under the CC-BY-NC-ND 4.0 license http://creativecommons.org/licenses/by-nc-nd/4.0/

(a) Fan for gas-air mixing inside the tank **(b) Fan for gas-air mixing outside the tank**

Fig. 5 Locations of fans for gas-air mixing

Two explosion-proof fans were used for the methane-air mixing. As demonstrated in Fig. 5(a), a fan and a recirculation pump were connected to the center tank to inflate and circulate air inside the tank, whereas another fan shown in Fig. 5(b) was used to mix the methane-air mixture in the space between the center tank and the film confined region. In order to ensure the homogeneity of the gas concentration inside the tank and the film confined region, approximately 20 min was required to inflate and mix methane and air. The gas concentration was measured by using an infrared methane analyzer, as seen in Fig. 6. The high speed camera and computer controlling system were located at about 25m away from the tank group, and the tanks with compressed gas were placed another 20m away from the high speed camera, as seen in Fig. 7. The resolution and shutter time of the HSVC were set at 2000–3000 fps and 1/50,000, respectively. Through-The-Lens (TTL) system was used to synchronize HSVCs with sensors. A 45m long gas pipe was used to supply methane from the compressed gas resources to the

© 2018. This manuscript version is made available under the CC-BY-NC-ND 4.0 license http://creativecommons.org/licenses/by-nc-nd/4.0/

testing tanks. The Gas Flow Control System (GFCS) used for methane-air gas filling and mixing is illustrated in Fig. 8.

The fan to mix methane and air for the center tank is shown in Fig. 9 (a), the fan has an air pump to drive the flow circulation. Two circulate ducts were connected with the center tank. However, in order to make the gas mixing procedure easier, the fan was placed outside the confined film region, as seen in Fig. 9 (b). The other fan used to mix methane and air inside the confined film region is shown in Fig. 9 (c). The gas mixing for the center tank and another gas mixing for the confined film region were conducted simultaneously. The air pump in the GFCS for gas concentration measurement is shown in Fig. 9 (d).

Once the gas filling started, the fans and air pump were activated to circulate the flow inside the center tank and the region confined by polyethylene films. During the gas filling procedure (about 20 mins), the air pump (Fig. 9 (d)) connected to the infrared gas concentration analyzer (Fig. 6) and the gas filled region was constantly used. A probe connected to the air pump as seen in Fig. 10 (a) was placed inside the confined film region by one person, while the other side of the air pump connected to the infrared gas concentration analyzer provided up-to-date gas concentration data. As shown in Fig. 10 (b), another person synchronously removed the fan for the center tank, and the probe was also used to measure the gas concentration inside the tank. When the gas concentration inside the tank reached the same level (9.5 vol %) of that inside the confined film region, the homogeneous gas mixture for the whole region was guaranteed. The hex nuts and rubber washers were then quickly installed to seal the valves on the tank wall after the measurement, as shown in Fig. 10 (b).

© 2018. This manuscript version is made available under the CC-BY-NC-ND 4.0 license http://creativecommons.org/licenses/by-nc-nd/4.0/

Fig. 6 Infrared gas concentration analyzer

Fig. 7 Location of high speed camera, computer system and compressed gas resources

© 2018. This manuscript version is made available under the CC-BY-NC-ND 4.0 license http://creativecommons.org/licenses/by-nc-nd/4.0/

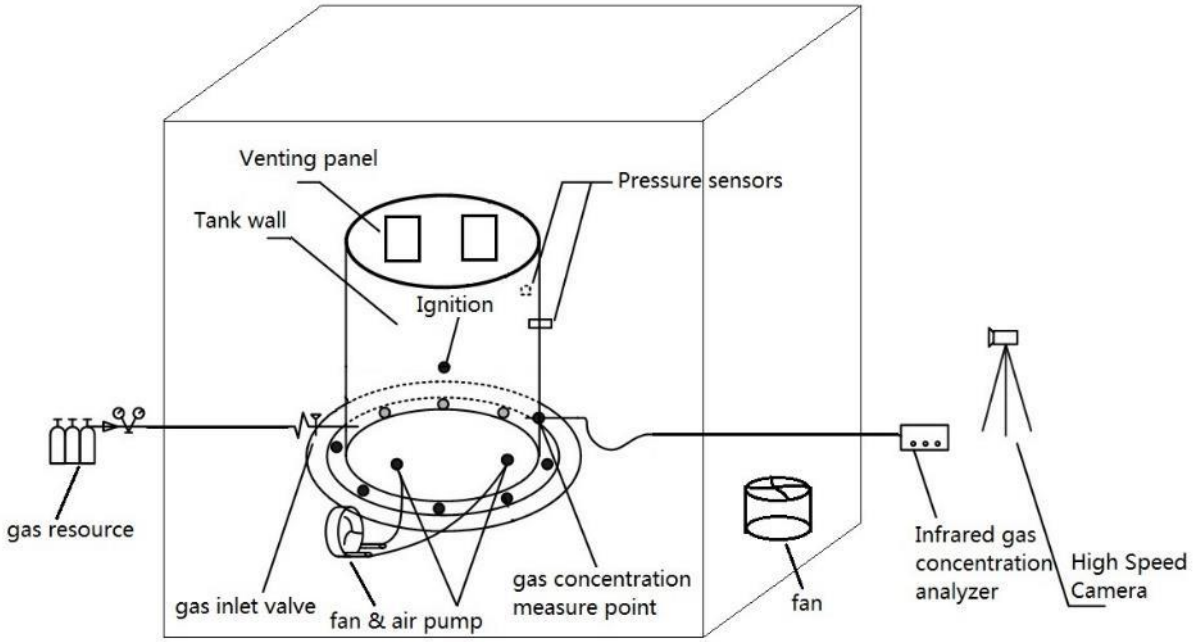

154

© 2018. This manuscript version is made available under the CC-BY-NC-ND 4.0 license http://creativecommons.org/licenses/by-nc-nd/4.0/

Fig. 8 Gas flow control system scheme

(a) Fan for gas mixing for the center tank **(b) Fan outside the confined film region**

(c) Fan for gas mixing for the confined film region **(d) Air pump**

Fig. 9 Detailed control units in the Gas flow control system scheme

© 2018. This manuscript version is made available under the CC-BY-NC-ND 4.0 license http://creativecommons.org/licenses/by-nc-nd/4.0/

(a) Measurement for the confined region **(b) Measurement for the tank after mixing**

Fig. 10 Methane-air mixture concentration measuring procedure

The ignition system was remotely activated once all personnel evacuated far away from the tanks. As shown in Fig. 8, an electric spark plug was installed in the middle of the center tank. Center ignitions were used for all gas explosion tests in this study. A water bucket was placed on the top of the truss to provide cold water to the water cooling system, as seen in Fig. 11. All sensors were connected to each other by using two water tubes, and fire-resistant coating was applied.

© 2018. This manuscript version is made available under the CC-BY-NC-ND 4.0 license http://creativecommons.org/licenses/by-nc-nd/4.0/

(a) Water bucket on top of the truss **(b) Water tubes to connect sensors**

Fig. 11 Water cooling system

2.2 Experimental layouts

As shown in Fig. 12, three tank group layouts, namely with separation gap 500mm, 750mm and 1000mm, were considered to study the effects of separation gap between tanks on blast wave propagation and interaction with the tank group. The center tank was fixed onto a concrete ground, which was built with normal-weight Portland cement concrete with a standard compressive strength equal to about 20 MPa. Each tank's weight was over 1.5 ton, overturning moment of tank due to recoil force was eliminated. In order to move the tanks to arrange different layouts, a crane truck as seen in Fig. 13 (a) was used. The final arrangement of the tank group is shown in Fig. 13 (b).

© 2018. This manuscript version is made available under the CC-BY-NC-ND 4.0 license http://creativecommons.org/licenses/by-nc-nd/4.0/

184

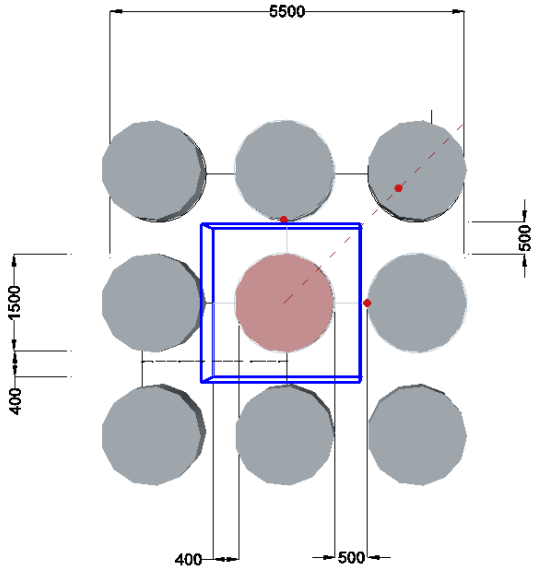

185

186 **(a) 500mm separation gap between tanks**

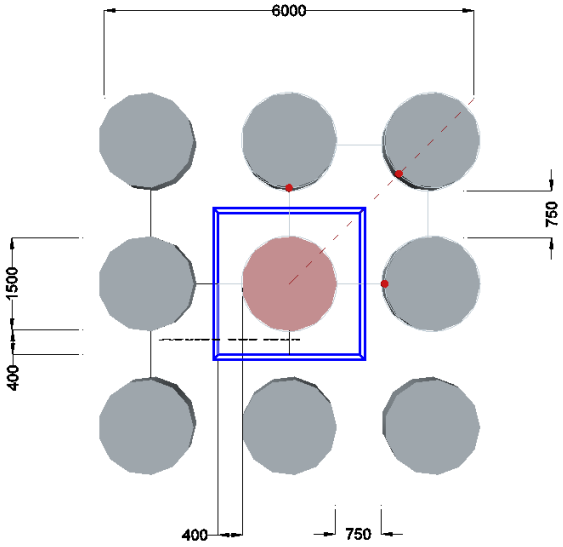

(b) 750mm separation gap between tanks

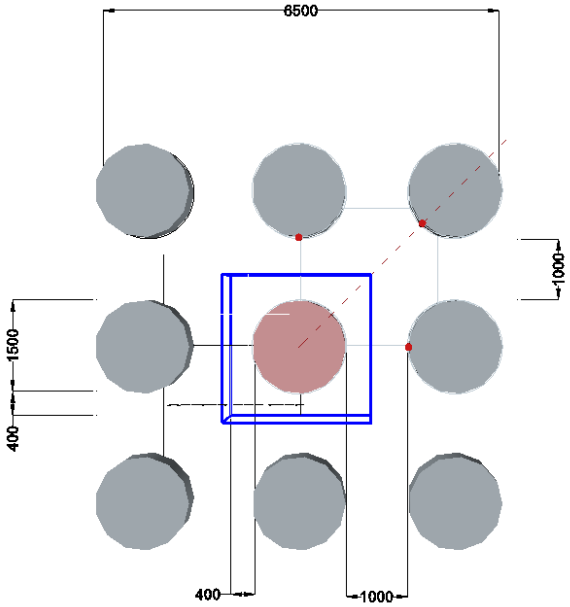

187

188 **(c) 1000mm separation gap between tanks**

189 **Fig. 12 Tank group layouts in methane-gas explosion testing**

190

© 2018. This manuscript version is made available under the CC-BY-NC-ND 4.0 license http://creativecommons.org/licenses/by-nc-nd/4.0/

(a) Hauling of tanks by using a crane truck to arrange the tank group layout

(b) Final tank group setup

Fig. 13 Tank arrangement for gas explosion testing

2.3 Experimental results and discussion

Before the tank group experiments in this study, the authors had conducted other experiments of vented gas explosions occurring inside the same-scale cylindrical tanks (Li et al., 2017). The uncertainties, such as gas concentration, vent activation pressure and roof failure pressure, etc., had been studied.

© 2018. This manuscript version is made available under the CC-BY-NC-ND 4.0 license http://creativecommons.org/licenses/by-nc-nd/4.0/

The tanks used in the authors' previous study (Li et al., 2017) were the same as the tanks used in this study, however, with different roofs and different venting areas. For different methane-air volume concentrations, the stoichiometric gas concentration of 9.5 vol % resulted in the greatest explosion overpressure. Therefore, 9.5 vol % was chosen in this study to investigate the worst scenario of methane explosions. As indicated in the previous study, different vent opening setups led to different initial activation pressures, which eventually resulted in errors in measuring the first and second pressure peaks. In order to minimize the experimental error, all roofs of the center tanks were uniformly designed to be venting cover free. In terms of the uncertainty of roof failure pressure, different welding procedures in the authors' previous study led to different roof failures. In the extreme case, the roof of the tank were propelled over 10 m from the tank. Therefore, in this study, in order to prevent the occurrence of the above scenario, continuous welds were used for all tank roofs. Furthermore, the uncertainty of the sensor recording accuracy was eliminated by ensuring the data from two sensors inside the tank wall were synchronized. However, due to the budget and number limitations of the tank group experiments, other uncertainties associated with the tank group tests were not further investigated.

High speed video camera was used to capture the flame propagation during combustion in the tests, as seen in Fig. 14. The stoichiometric methane-air concentration of 9.5 vol % was used for all testing cases. Two sensors were installed on the center tank wall to record internal pressures. One sensor with pressure measuring range of 0 to 30kPa was mounted on one side of the center tank, as illustrated in Fig. 11 (b), whereas the other sensor with pressure measuring range of 0 to 150kPa was installed on the opposite side of the tank. During the test, signals from these two sensors were recorded by using a data acquisition instrument at a fixed sampling frequency of 100 kHz. The unfiltered raw data were shown in Fig. 15. The repeated experimental setups with the same sensors and data acquisition system were used for three

© 2018. This manuscript version is made available under the CC-BY-NC-ND 4.0 license http://creativecommons.org/licenses/by-nc-nd/4.0/

different separation gap cases (namely 500mm, 750mm, and 1000mm cases). The raw data were obtained by two pressure sensors at two different locations inside the tank. Both sensors worked properly and were synchronized that pressure-time profile of sensor 1- coincided with that of sensor 1+, which guarantees the repeatability and sensitivity of the collected data. However, high frequency noises were observed for all the recorded data. To remove the measurement noise, the Fast Fourier transform (FFT) method of data filtering was used, 1000 Hz low pass filter was chosen for all testing results. Additionally, in order to compare with the CFD simulation data in the following section, the starting times of raw data were adjusted to zero.

For demonstration purpose, only the recorded images with the 500mm separation gap was chosen to discuss the combustion progress. Four high speed video camera snapshots were shown in Fig. 17 for the explosion testing with 500mm separation gap, the corresponding timelines were indicated in the pressure-time curves of the internal sensor (i.e. sensor 1+), as seen in Fig. 16. The pressure-time data were filtered and compared with originally recorded data.

(a) 500mm separation gap (b) 750mm separation gap (c) 1000mm separation gap

Fig. 14 High speed video camera snapshots of different separation gap scenarios in gas explosion testing

© 2018. This manuscript version is made available under the CC-BY-NC-ND 4.0 license http://creativecommons.org/licenses/by-nc-nd/4.0/

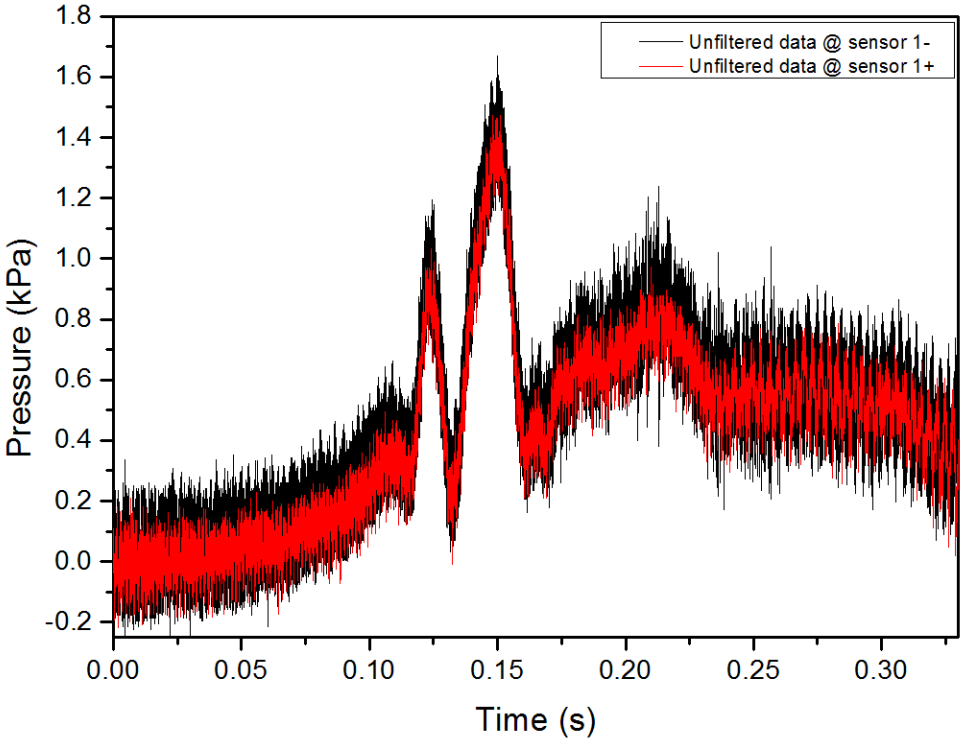

245

246 **(a) Unfiltered raw data recorded by the two internal sensors for 500mm case**

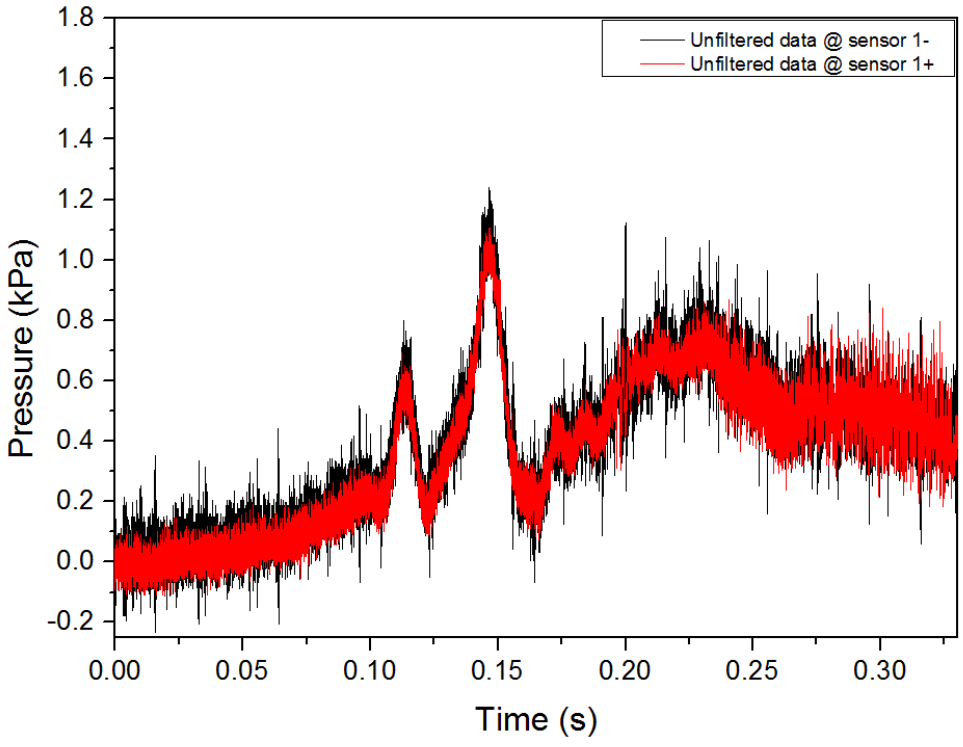

247

248 **(b) Unfiltered raw data recorded by the two internal sensors for 750mm case**

© 2018. This manuscript version is made available under the CC-BY-NC-ND 4.0 license http://creativecommons.org/licenses/by-nc-nd/4.0/

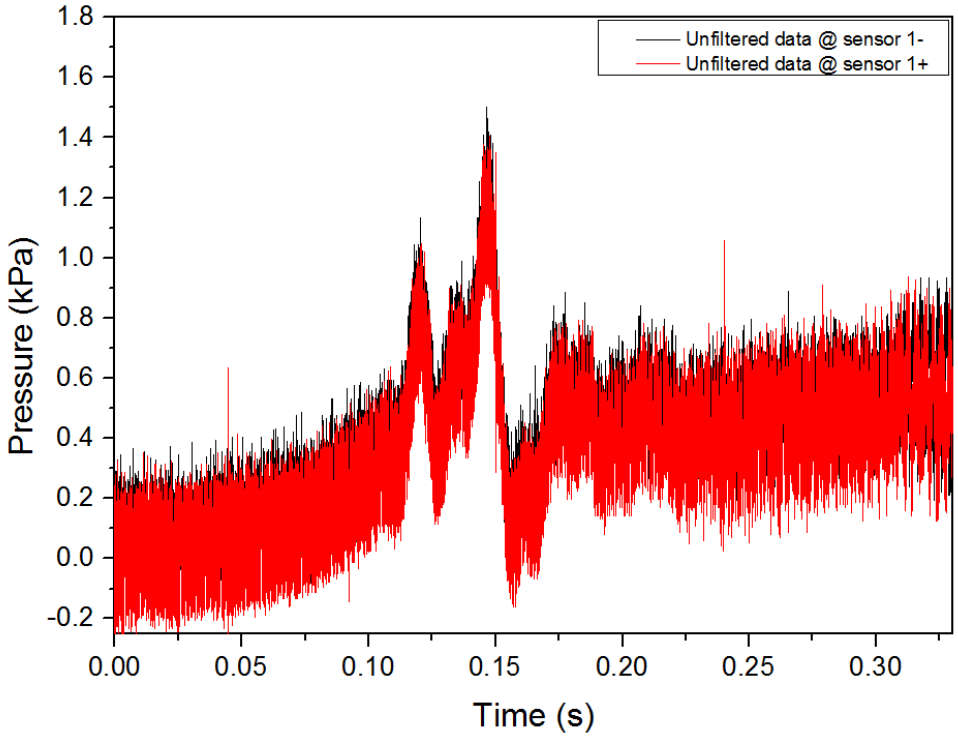

(c) Unfiltered raw data recorded by the two internal sensors for 1000mm case

Fig. 15 Unfiltered raw data of internal overpressures for all separation gap cases

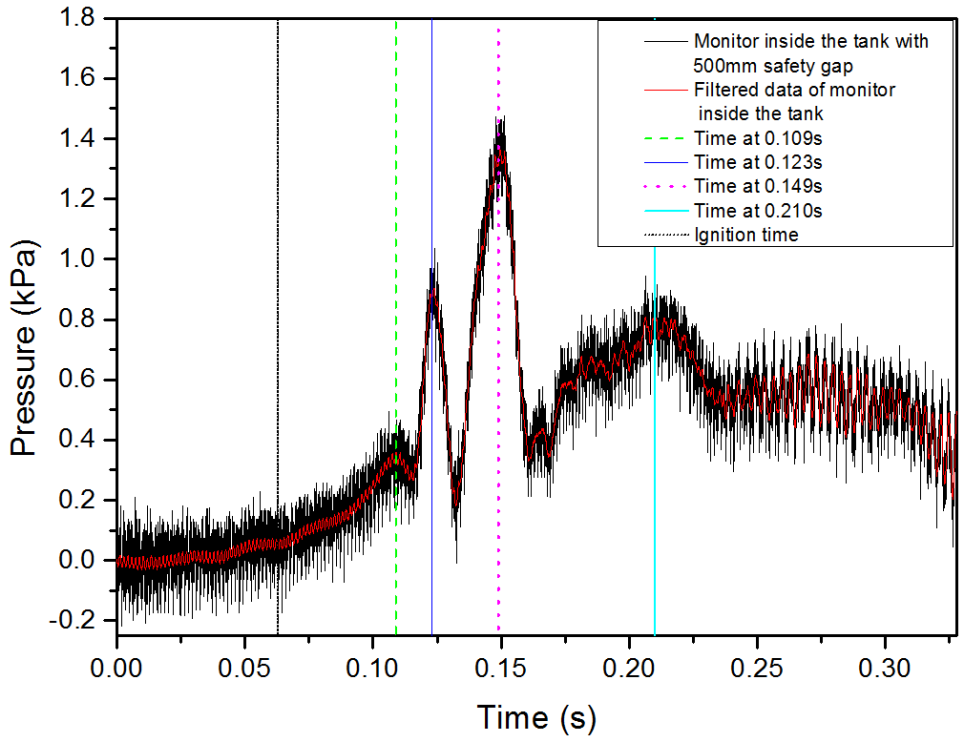

Fig. 16 Filtered internal pressures with timelines for center tank with 500mm separation gap

© 2018. This manuscript version is made available under the CC-BY-NC-ND 4.0 license http://creativecommons.org/licenses/by-nc-nd/4.0/

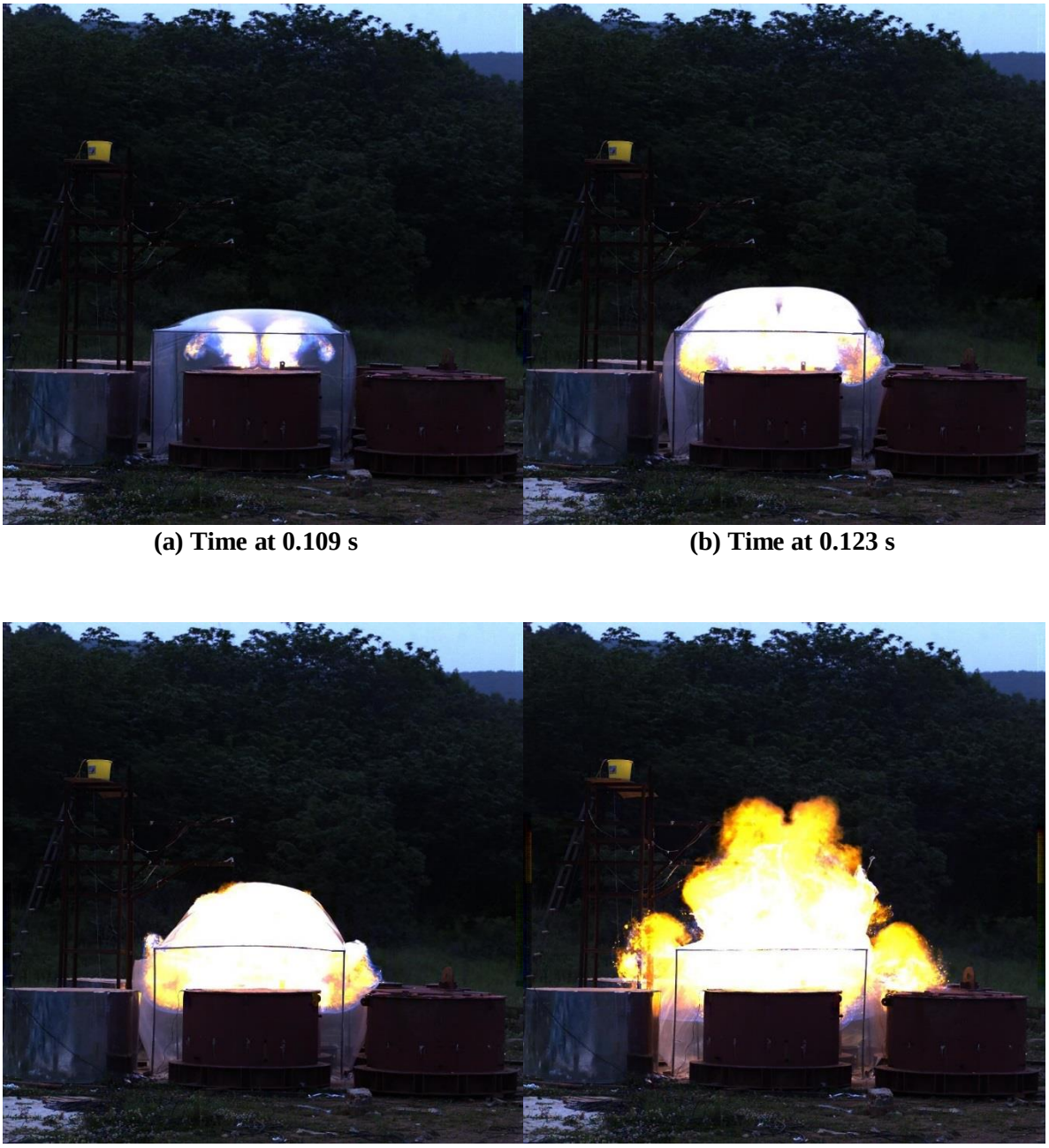

(a) Time at 0.109 s **(b) Time at 0.123 s**

(c) Time at 0.149 s **(d) Time at 0.210 s**

Fig. 17 High speed video camera snapshots for tank group with 500mm separation gap

The center tank had two openings without panels, while the outer region (dimensions of 2300×2300×1500 mm^3) was fully confined by using a polyethylene film. From the time of ignition to the time that the confined rectangular region was filled with unburned gas escaped from the center tank, the flame front inside the tank expanded spherically. During this time frame, the combustion resulted in a net rate of volume production exceeding the flow rate of unburned gas from the vent. Therefore, as seen in Fig. 16 (from ignition time to 0.109), the

© 2018. This manuscript version is made available under the CC-BY-NC-ND 4.0 license http://creativecommons.org/licenses/by-nc-nd/4.0/

internal pressure increased. An obvious pressure decrease was not seen due to the fact that the failure pressure of tank panel was zero (i.e. two openings were not confined). The outflow of unburned methane-air mixture from the vent opening eventually distorted the flame front (Fig. 17 (a)). Consequently, low density burnt product during the combustion inside the tank was expelled due to the distorted flame front, which resulted in an increase in the flow. Such flow speed increased along with the expansion of the film confined volume until some gas leakage occurred through the film, resulting in a slight fall in the internal pressure, as seen in Fig. 16 (from time of 0.109 s to the trough before time of 0.123 s).

From Fig. 17 (a) to Fig. 17 (b), the flame front ignited the unburned methane-air mixture concentrated within the confined rectangular region, which led to a sharp increase in the internal pressures, as the second peak pressure shown in Fig. 16 at 0.123 s. Starting from 0.123 s, the sideward polyethylene film on the edge of the confined region broke. A sudden pressure drop was hence observed due to the failure of film from time 0.123 s to time 0.131 s. However, the film located on the top of the confined area did not burst until the time of 0.149 s. During this time the external explosion within the confined region continued so that the flame surface area increased till the second failure of the film, which leaded to another pressure decline. A third pressure spike was subsequently seen at 0.149 s.

From 0.149 s, the onset of burned methane-air mixture after the failure of all films coincided with oscillatory combustion. Meanwhile, burning velocities were enhanced by turbulence generated between burned and unburned mixture within the center tank. The induced flame acceleration was also boosted due to the turbulence interacted with the center tank and surrounding tanks. The methane-air mixture density interface became unstable during the flame acceleration, and Taylor instabilities (Bauwens et al., 2010; Bauwens et al., 2011; Cooper et al., 1986) were expected. The growth of such instability and oscillation was seen between 0.149 s and 0.210 s in Fig. 16. The fourth pressure peak was observed at time of 0.210 s when the

© 2018. This manuscript version is made available under the CC-BY-NC-ND 4.0 license http://creativecommons.org/licenses/by-nc-nd/4.0/

flame area inside tank reached the maximum and encountered the tank walls. The burned mixture then had a decreasing rate of production from 0.210 s due to the reduction of flame area in later stage of combustion. However, the last pressure peak due to acoustic effect (Cooper et al., 1986; Tamanini and Chaffee, 1992; Van Wingerden and Zeeuwen, 1983) was not observed in this explosion test.

In Fig. 18, the pressure-time histories of the case with 500mm separation gap were compared with the other cases with the separation gap 750mm and 1000mm. As seen in the zoomed-in figure on the right corner of Fig. 18, the burning velocity of the gas mixture was reflected by the pressure increase rate in the highlighted triangle area. All pressure increase rates coincided with each other, indicating the laminar burning velocities for all cases were the same. In other words, the measuring and mixing of stoichiometric methane-air concentration (i.e. 9.5 vol %) in all tests were accurate.

In the comparison, 500mm case showed the greatest pressure peaks before the 0.161 s, while 750mm case had the smallest pressure peaks. However, after 0.161 s, a more regular pattern was seen that the change of separation gap distance from 500mm to 1000mm was inversely proportional to the fourth pressure peaks. Namely, the increase of the separation gap distance resulted in a decrease of the peak pressures at 0.210 s. The observed irregular pressure peak patterns before 0.161 s were due to the discreteness of the film failure. As explained before, the first three pressure falls were highly relevant to the failure pressure of the polyethylene film, which was unfortunately not controllable in the tests. The peak pressure appeared nearly immediately after the film breaks, especially for low pressure combustions in these tests. After 0.161 s all films were burned, the influence of turbulence within the tank and between tanks became more obvious. With a closer separation gap distance, the center tank had larger flame turbulence interaction with the adjacent tanks. The higher turbulence eventually resulted in higher pressure feedback to the internal pressures (Li et al., 2016; Ma et al., 2014). Therefore,

© 2018. This manuscript version is made available under the CC-BY-NC-ND 4.0 license http://creativecommons.org/licenses/by-nc-nd/4.0/

316 a decrease tendency of pressure peaks at 0.210 s was seen when the separation gap distance
317 proportionally increased from 500mm to 1000mm.

318 Table 1 summarizes all the external sensors' locations and the recorded peak pressures. The
319 pressure-time histories obtained by the four external sensors are shown in Fig. 19. It is seen in
320 Fig. 19 (a) and (b) that increasing the separation gap distance from 500mm to 1000mm leaded
321 to smaller maximum peak pressures at sensor 2 and sensor 3. The external pressures at the these
322 two locations were more influenced by the turbulence generation. The narrower separation gap
323 induced higher turbulence between the tanks. Therefore, the comubustion within the 750mm
324 gap developed higher peak overpressure than that of 1000mm gap case, even though the
325 internal pressure from the explosion center for 750mm gap case was initially lower than that
326 of 1000mm gap case. However, for other sensors (i.e. sensor 4 and sensor 5) located above the
327 vent opening, the external peak pressure development tendencies were the same as that of the
328 internal peak pressure shown in Fig. 18. The above observation can be explain as: during the
329 vented explosion, the high velocity flame impinged out of the vent vertically with consequent
330 turbulence generated spherically. The impulse and pressure due to venting were more dominant
331 in the vertical direction, and the obstacle/confinement ratio in this direction was unchanged
332 regardless of the variation of separtion distance. Whereas the majority of turbulence developed
333 horizontally due to the changed obstacle ratio which was related to the changed separation
334 distance. Unlike the turbulence influenced sensors in Fig. 19 (a) and (b), the pressures recorded
335 by sensor 4 and sensor 5 above the vent were mainly subjected to the venting pressure with
336 little turbulence ration. Therefore, the internal pressure of changing tendencies shown in Fig.
337 18 directly affected those recorded by sensors 4 and 5 as shown in Fig. 19 (c) and (d).

338 It is also worth noting that the oscillations of pressures after the peak pressures (at 0.151 s and
339 0.152 s) for sensor 4 and sensor 5 became more obervious than the data recorded at sensor 2
340 and sensor 3. Sensor 4 and sensor 5 are external sensors outside the tank in the venting direction.

© 2018. This manuscript version is made available under the CC-BY-NC-ND 4.0 license http://creativecommons.org/licenses/by-nc-nd/4.0/

The peculiar profiles with strong oscillations are mainly due to the locations of these two sensors. Unlike sensor 2 and sensor 3 which were installed on the neighbouring tank walls far away from the vent, sensor 4 and sensor 5 were directly subjected to the hot flame since the beginning of combustion. Therefore, sensor 4 and sensor 5 had longer exposure time to high temperature heat. Moreover, sensor 2 and sensor 3 were better-protected against wind within the tank group while sensor 4 and sensor 5 were not confined in the open air. In such a scenario, sensor 4 and sensor 5 became more sensitive, especially under longer time of hot flame exposure. More importantly, the pressure profiles of internal sensor 1 in Fig. 18 has strong oscillations between 0.15 s and 0.30 s, such oscillations are undoubtedly mapped to the recorded data in Fig. 19 (c) and (d).

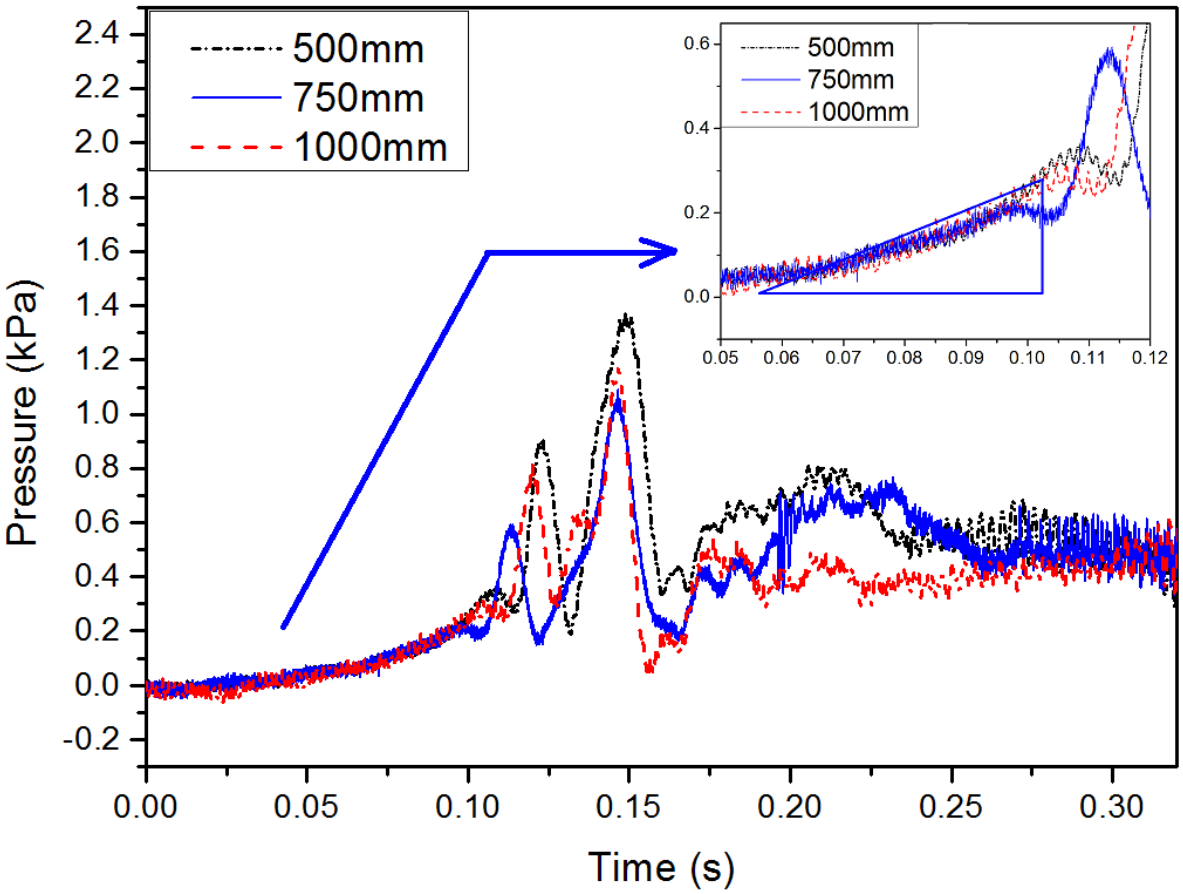

Fig. 18 Pressure-time histories recorded inside the center tank with different separation gaps

© 2018. This manuscript version is made available under the CC-BY-NC-ND 4.0 license http://creativecommons.org/licenses/by-nc-nd/4.0/

353 **Table 1 Sensor locations and measured peak pressures.**

Sensor No.	Sensor location	*Tank*	Measured peak pressure for 500mm case (kPa)	Measured peak pressure for 750mm case (kPa)	Measured peak pressure for 1000mm case (kPa)
1-	Internal wall @ W-direction	Center tank	1.375	1.080	1.177
1+	Internal wall @ E-direction	Center tank	Same as 1-	Same as 1-	Same as 1-
2	External wall @ W-direction	West tank	0.632	0.553	0.470
3	External wall @ SW-direction	South-West tank	0.442	0.326	0.289
4	1500mm above the center tank	Center tank	0.545	0.391	0.423
5	2000mm above the center tank	Center tank	0.451	0.278	0.332

354

355

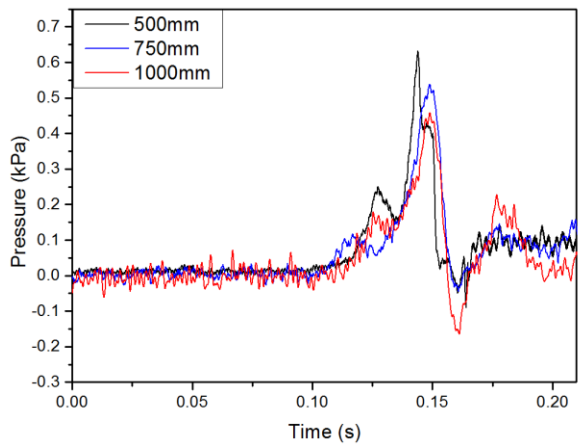

356

357 **(a) Sensor 2**

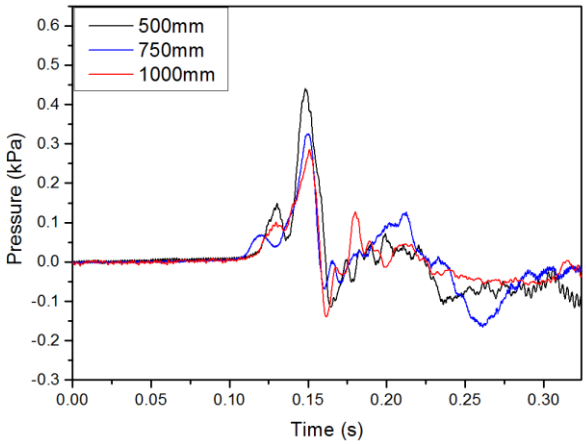

(b) Sensor 3

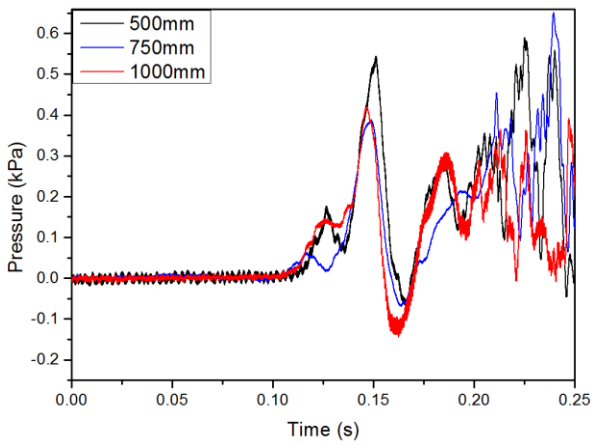

358

359 **(c) Sensor 4**

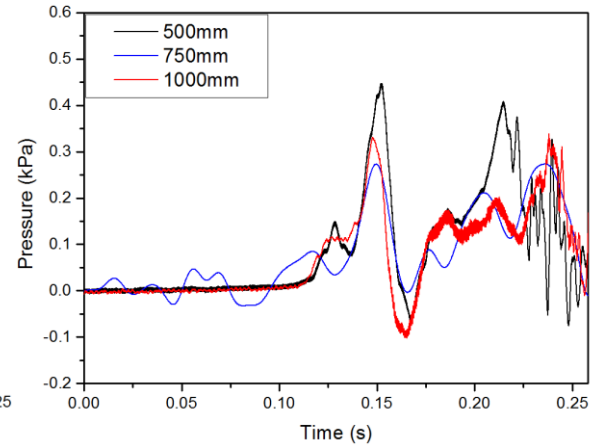

(d) Sensor 5

© 2018. This manuscript version is made available under the CC-BY-NC-ND 4.0 license http://creativecommons.org/licenses/by-nc-nd/4.0/

Fig. 19 Pressure-time histories recorded at different locations outside the center tank with different separation gaps

So far, only three experimental gas explosion tests were conducted. Due to the high cost of field explosion tests, a systematical investigation of separation gap effect on LNG tanks with more tests became infeasible. Therefore, further study was conducted by using CFD simulations, the overpressure generations inside and outside the vented tank were studied in the following sections.

3 CFD simulation and validation

Following the authors' previous study on vented methane-air explosion overpressure calculation (Li et al., 2017), the same CFD-based software FLACS (version 10.4) was used in this paper. FLACS uses Navier-Stokes equations and k–ε model for turbulence simulation. Obstacles and walls in complex three-dimensional geometries are represented by using on-grid and sub-grid objects with computed porosity values. The database of chemical kinetics, momentum, energy balance equations, and special schemes for flame velocity and turbulence calculation are included (Arntzen, 1998; Ferrara et al., 2006; Hjertager, 1984, 1993). In FLACS, the combustion models for gas explosion simulation include BETA flame model and Simple Interface Flame (SIF) model, while for fire simulation, Eddy Dissipation Concept (EDC) is recommended. The SIF model, which was commonly used in vented or highly confined gas explosion studies (Bleyer et al., 2012; Li and Hao, 2017; Li et al., 2017; Vyazmina and Jallais, 2016), was employed in this study. SIF model solves compressible flows by modelling flame as an interface to ensure good representation of flame area in a coarse grid.

3.1 Vented explosion simulation of tank group by using FLACS

The experimental setup as seen in Fig. 13 was numerically modelled in FLACS. Fig. 20 shows the 3D geometry of the tank group with grid cells. The entire simulation domain dimensions were 18000×18000×18000 mm^3. For each tank with dimensions of 1500mm diameter and

© 2018. This manuscript version is made available under the CC-BY-NC-ND 4.0 license http://creativecommons.org/licenses/by-nc-nd/4.0/

1000mm height, the distance from the tank to the external boundaries in non-venting direction (horizontal direction) is about 4 times larger than tank diameter. The distance from the tank to boundary is 18 times larger than tank length in explosion venting direction. Therefore, the requirement of distance from vessel to boundaries for vented gas explosion in FLACS was met (Gexcon, 2015). A non-reflecting boundary condition of "PLANE_WAVE" was used. This boundary condition was designed to reduce the reflection of the pressure waves at open boundaries. The pressure wave reflection is caused by setting a fixed pressure at the boundary. The PLANE_WAVE boundary condition extrapolates the pressure in such a way that reflections are almost eliminated for outgoing waves. The PLANE_WAVE boundary condition is recommended for explosions in low confinement and for far field blast propagation (Gexcon, 2015).

The grid cell size within the combustion region (about 4000×4000×4000 mm^3) was chosen as 0.05m (Li and Hao, 2017; Li et al., 2017), and all grid cells were modelled as cubical inside the enclosure to reduce the deviations of burning velocity and pressure development. About 70 grids, which are much higher than required 8 grids in FLACS manual (Gexcon, 2015), were used at each vent opening. Other grid cells were stretched from the combustion region to external boundaries, the aspect ratio of grid increase was kept as 4%. Tank walls and roofs were assumed as rigid in all simulation. Ambient temperature of 26^{o}C, which is approximately the same as the outdoor temperature in the field during the tests, was used, as well as the wind speed of 2.8 m/s. Atmospheric pressure of 1 ATM was adopted. The volume concentration of methane-air mixture was kept as stoichiometric at 9.5 vol%.

In order to emulate the lightweight film used in experiments, the PLASTIC relief panel was chosen in FLACS. An UNSPECIFIED panel type was initially created, and the area-porosity, density and opening pressure were adjusted to meet the PLASTIC panel properties. It is seen in Fig. 20 (b) that the monitoring points (green points) were located at the same positions as

© 2018. This manuscript version is made available under the CC-BY-NC-ND 4.0 license http://creativecommons.org/licenses/by-nc-nd/4.0/

411 the sensors in the experimental setup, except that two extra monitors (i.e. sensor 6 and sensor
412 7) were added to record sideward and external pressures inside and outside the tank group in
413 non-venting direction. Sensor 6 and sensor 7 were fixed at the location about 1.1 m in vertical
414 and 1.1 m in horizontal direction from the group center, while sensor 2 and sensor 3 attached
415 on the adjacent tank walls move as the tanks were relocated in each case with different
416 separation distances. The ignition, as shown in Fig. 20 (b), was located in the middle of the
417 center tank.

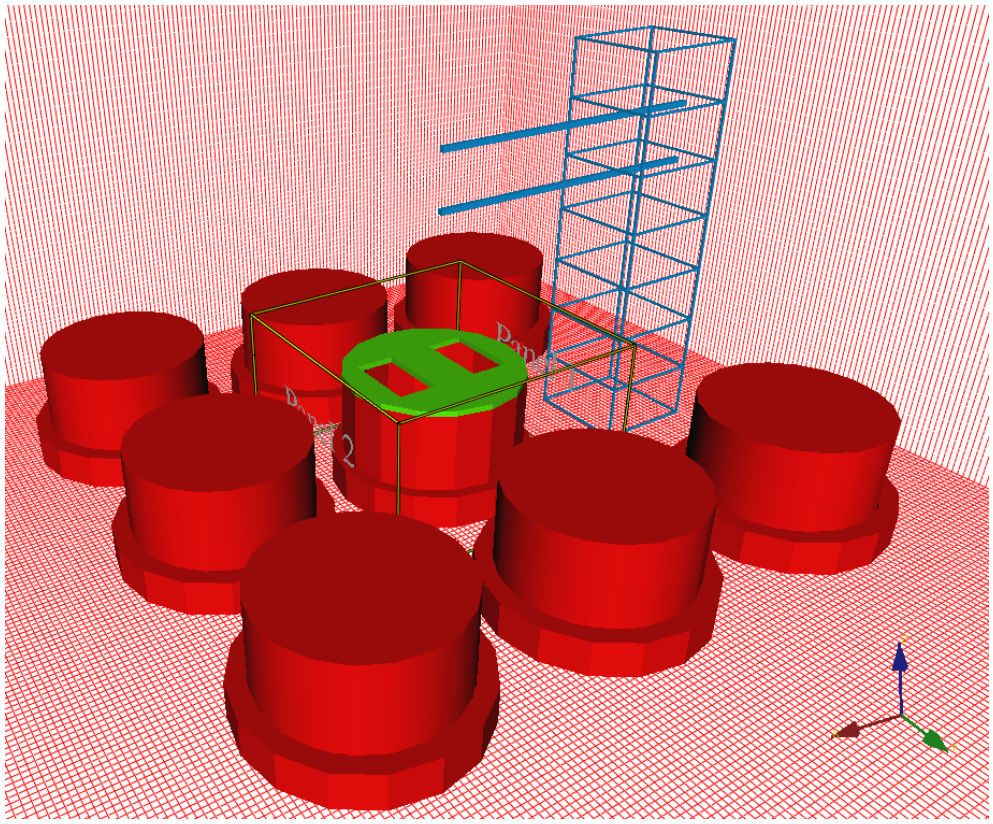

418

419 **(a) 3D geometry and grid cells**

© 2018. This manuscript version is made available under the CC-BY-NC-ND 4.0 license http://creativecommons.org/licenses/by-nc-nd/4.0/

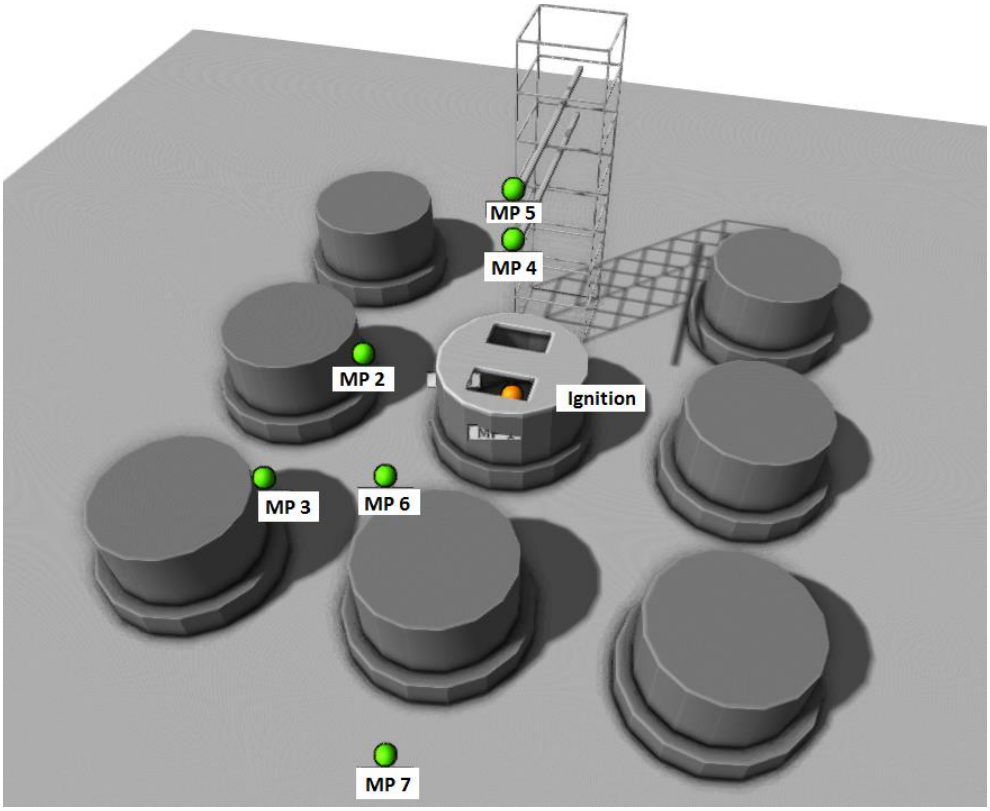

420

421 **(b) Monitor locations**

422 **Fig. 20 3D model of the tank group in FLACS simulation**

423

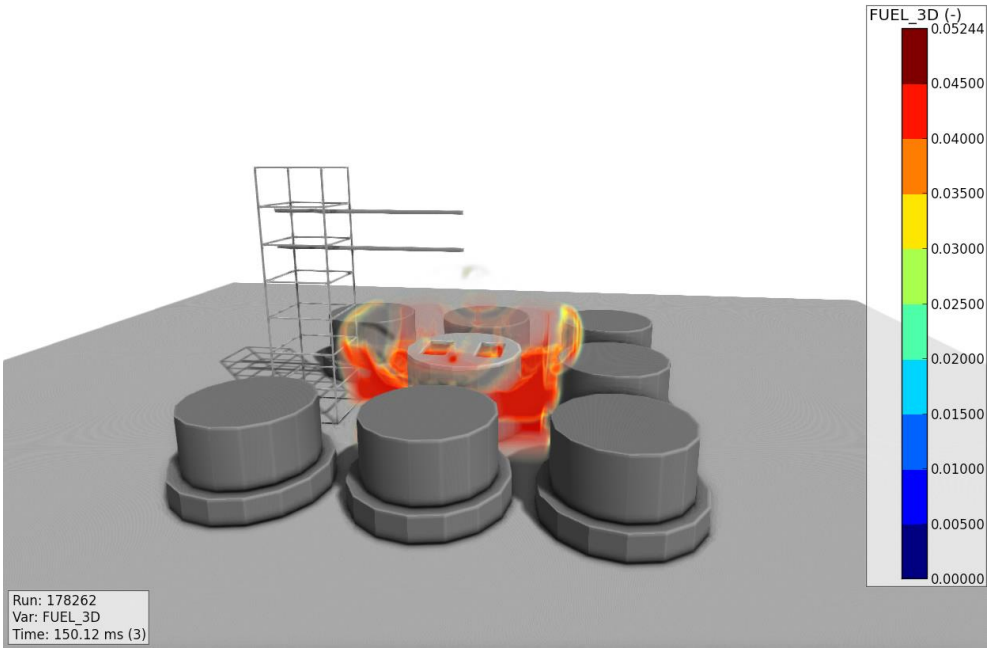

424

425 **(a) Separation gap distance of 500mm**

© 2018. This manuscript version is made available under the CC-BY-NC-ND 4.0 license http://creativecommons.org/licenses/by-nc-nd/4.0/

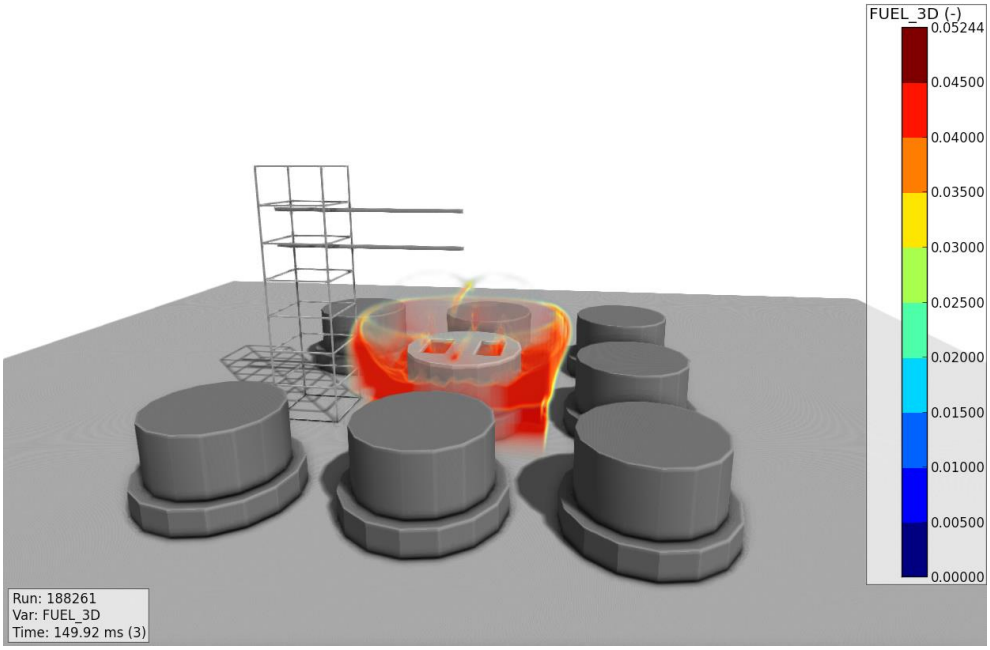

(b) Separation gap distance of 750mm

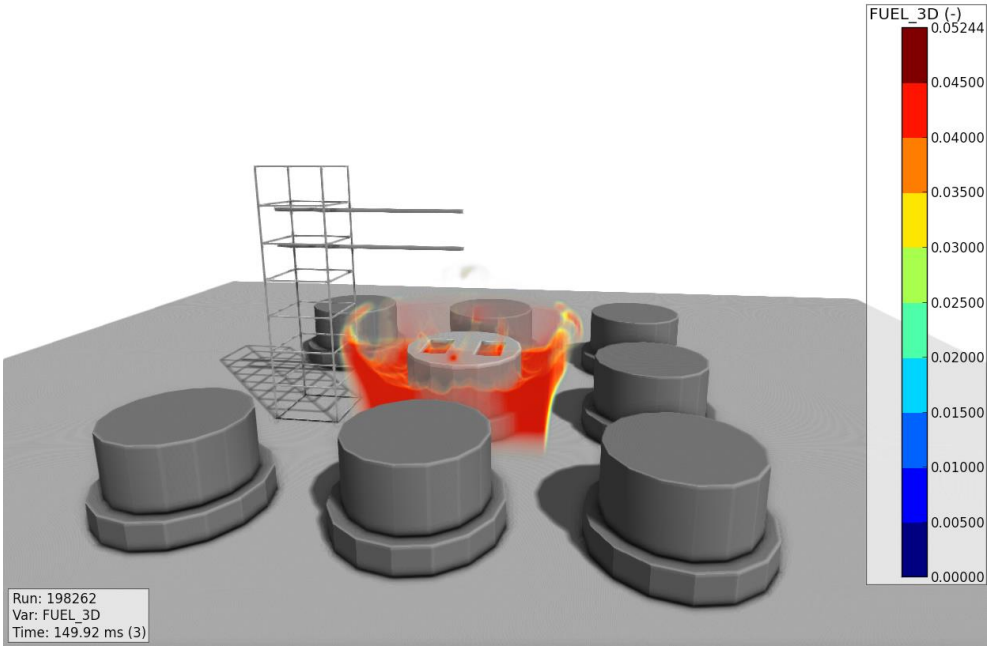

(c) Separation gap distance of 1000mm

Fig. 21 3D modelling of combustion by using FLACS

3.2 Comparison of internal and external overpressures predicted by FLACS with experimental data

Corresponding to the combustion progress as shown in Fig. 14 and Fig. 17, the three-dimensional modellings of three different vented explosion scenarios in FLACS were well

© 2018. This manuscript version is made available under the CC-BY-NC-ND 4.0 license http://creativecommons.org/licenses/by-nc-nd/4.0/

captured as shown in Fig. 21. All overpressure-time history data were extracted from different monitors in FLACS, as shown in Fig. 22 and Fig. 23. In comparison of the internal pressures in Fig. 22, the first pressure peak and the maximum pressure peak were well predicted. The Taylor instability induced pressures after the maximum pressure peak (at 0.149 s in experiment and at 0.121 s in FLACS CFD simulation) were also well observed, even though the difference between the Taylor instability induced pressures in experiments were more obvious than that in CFD simulation. In both pressure-time curves, the 500mm separation gap scenario had larger pressure peaks, whereas the lowest third pressure peaks were observed in the 1000mm separation gap scenario. Generally, FLACS well predicts the amplitude of pressures and the general shapes of dominant peaks of pressures inside the center tank. Except that the pressure build-up in FLACS started sooner than that in experiments, which is due to the fact that the initial burning rate of flame in FLACS simulation was slightly faster. Such phenomenon had also been observed in other researchers' studies (Ma et al., 2014; Pedersen and Middha, 2012).

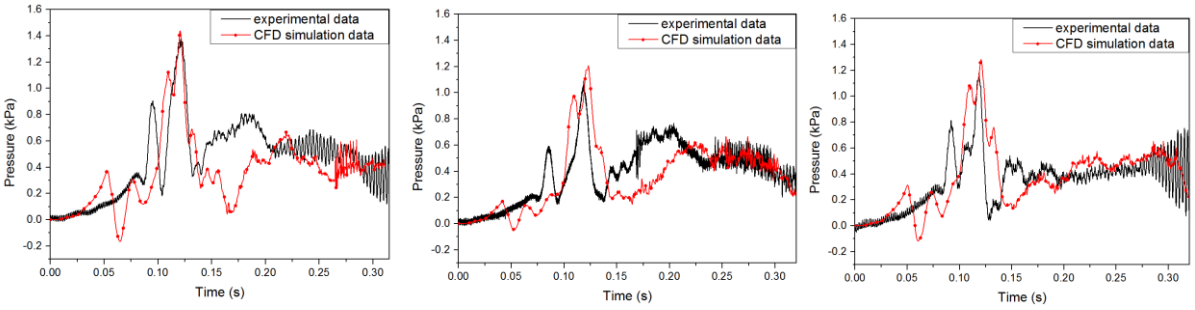

(a) Data of 500mm case **(b) Data of 750mm case** **(c) Data of 1000mm case**

Fig. 22 Comparison of experimental and CFD data of internal pressures recorded at monitor 1

The earlier pressure build-up was also applied onto other obtained external pressures as seen in Fig. 23. The majority of the external pressure peaks in FLACS agrees well with the experimental data. At monitor 2 and monitor 3, the decline tendency of the maximum pressure with the increase in separation gap was well predicted. Whereas the differences among the maximum pressures subjected to different separation gaps were not obviously seen at monitor

© 2018. This manuscript version is made available under the CC-BY-NC-ND 4.0 license http://creativecommons.org/licenses/by-nc-nd/4.0/

4 and 5 in FLACS. Additionally, the agreement of Taylor instability induced pressures and negative pressures between FLACS and experiments is satisfactory, despite the fact that the recorded pressure oscillations in the test at monitor 4 are much higher than CFD predicted data. As explained before, the explosion was vented from two vent openings, the sensor 4 was in direct contact with the combustion products. The signal of pressure acquisition was highly likely being affected by the high temperature heat of the vented combustion.

According to the data in Fig. 23, it is again suggested that the increase of separation gap resulted in a decrease of the maximum pressures at monitor 2 and monitor 3. The turbulence generation between narrower tank gaps significantly increased the external pressures recorded at the above two monitors. Although the initial internal pressure inside the tank of 1000mm gap case was greater than that of 750mm gap case, the explosion occurred within the 750mm gap eventually induced greater turbulence, thereby generating higher pressures. However, different pressure development tendencies were seen at monitor 4 and monitor 5. In the CFD data, little differences among the pressure peak due to the effect of separation gap were seen. The spherically generated turbulence experienced zero obstacle/confinement ratio change in the venting direction whereas the separation gap exclusively varied in horizontal direction. Therefore, due to the little influence of turbulence in venting/vertical direction, the pressure peak changes recorded at monitor 4 and monitor 5 were negligible.

All the maximum pressures are summarized in Fig. 24. Generally, FLACS simulation results have a good agreement with experimental results, although pressure peaks were slightly over-predicted.

© 2018. This manuscript version is made available under the CC-BY-NC-ND 4.0 license http://creativecommons.org/licenses/by-nc-nd/4.0/

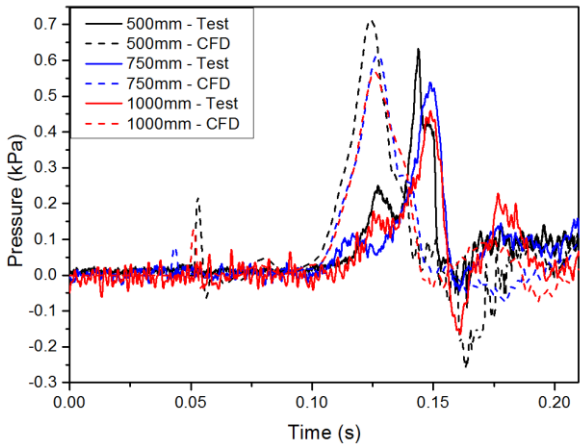

480

481 **(a) Monitor 2**

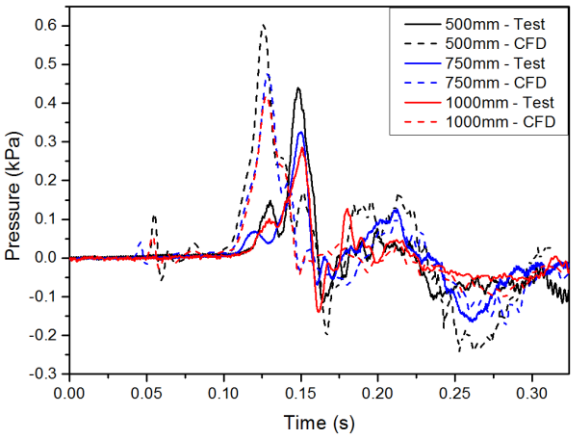

(b) Monitor 3

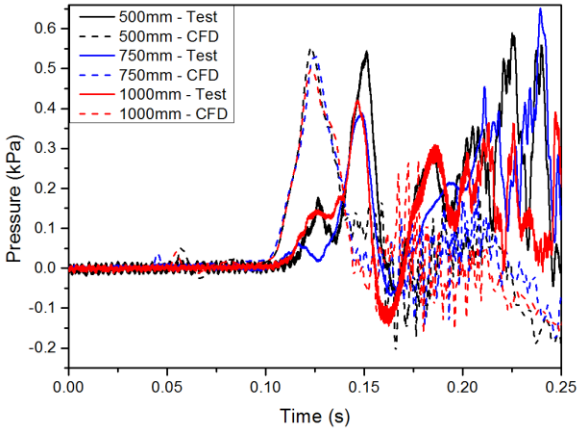

482

483 **(c) Monitor 4**

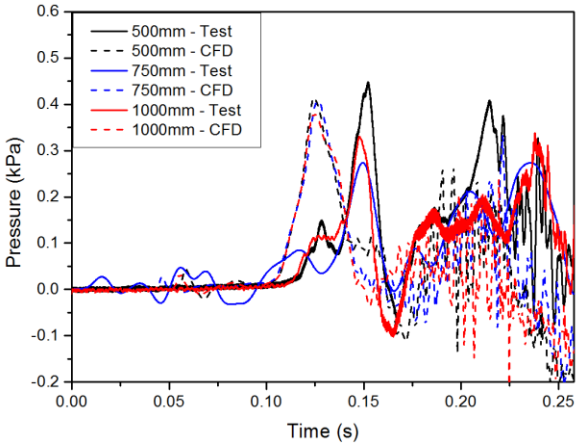

(d) Monitor 5

484 **Fig. 23 Comparison of test and CFD data of external pressures recorded at different monitors**

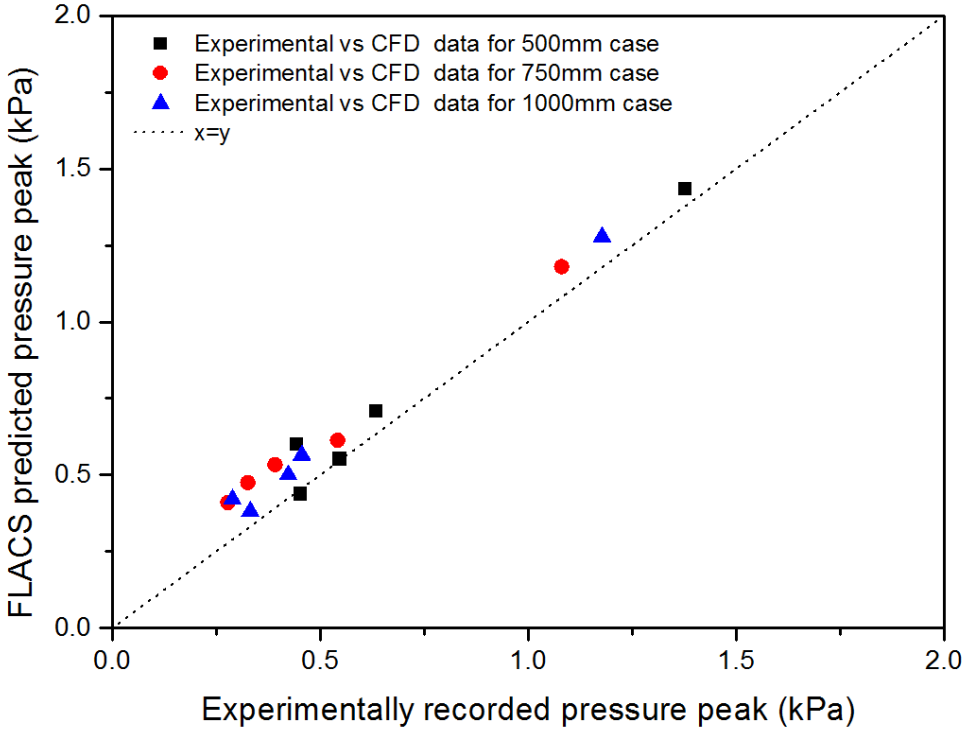

485

© 2018. This manuscript version is made available under the CC-BY-NC-ND 4.0 license http://creativecommons.org/licenses/by-nc-nd/4.0/

Fig. 24 Comparison of peak pressures recorded in the tests and CFD simulations at all monitor locations

In order to further validate the accuracy of FLACS in vented gas explosion overpressure prediction. The experiments regarding explosion in vented cylindrical tanks from Moen et al. (1982) were used to compare with FLACS simulation results in this study. In the experiments by Moen et al. (1982), the large combustion tanks with dimensions of 10m long and 2.5m diameter were segregated into different confined regions by using orifice plates, as shown in Fig. 25.

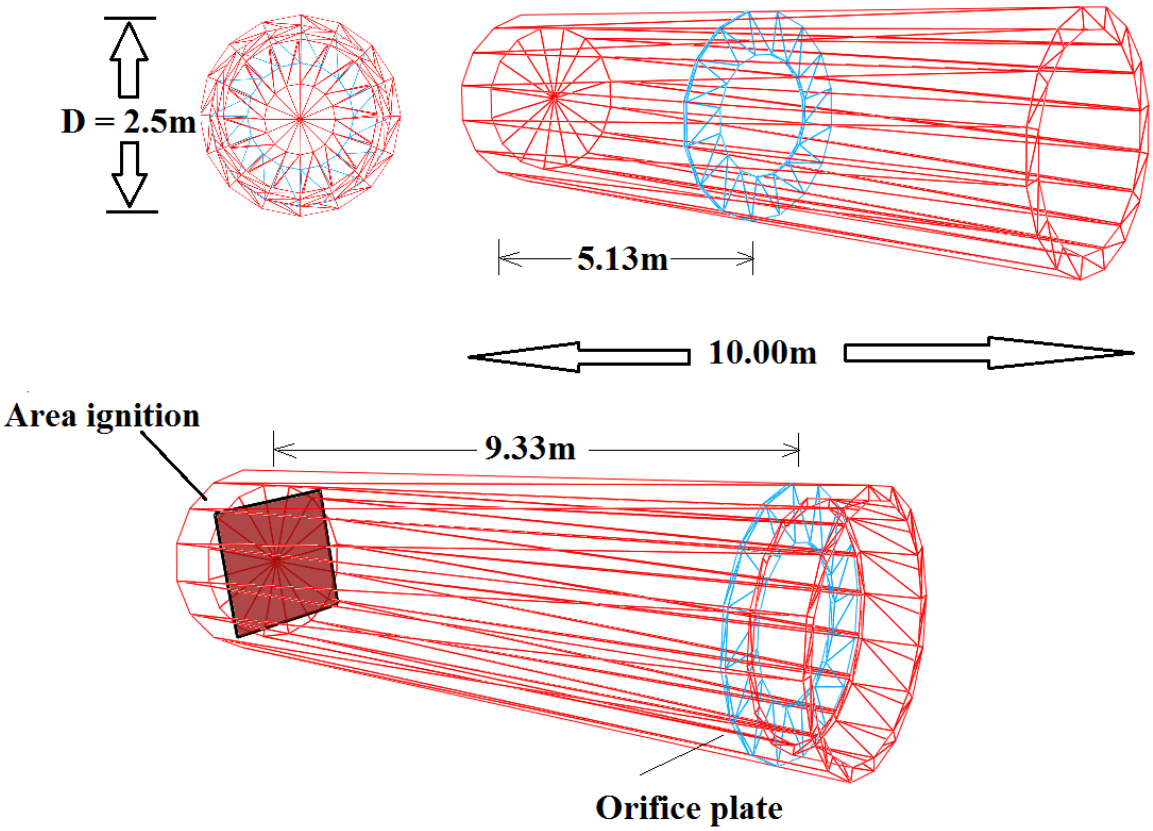

Fig. 25 Vented methane-air explosion configuration by Moen et al. (1982) modelled in FLACS

The left end of the tank was closed and area ignition was applied on this side, whereas the tank was open on the right side. The volume of the segregated region was defined as the cross section area times the distance from ignition to the orifice plate. The orifice plate were placed at

© 2018. This manuscript version is made available under the CC-BY-NC-ND 4.0 license http://creativecommons.org/licenses/by-nc-nd/4.0/

different locations (from 1.65m to 9.33m away the ignition), therefore, different confined volumes were defined. The orifice plates had different blockage ratios ($B.R. = 1-(d/D)^2$), which can be used to represent the different vent area ratio. 9.5 vol % methane-air mixture was also used. All the previous FLACS setups were kept the same.

The experimental setup information, peak pressure data and FLACS simulation data were summarized in Table 2. It is seen that the FLACS simulation data of peak pressures satisfactorily agree with experimental data (Moen et al., 1982), indicating FLACS can accurately simulate the methane-air explosion from vented single tank as well.

Table 2 Comparison of experimental results by (Moen et al., 1982) and and numerical results

Case ID.	Orifice plate (OP) distance from ignition	*Blockage ratio* of OP	Volume of confined region (m^3)	Peak pressure from experiments (kPa)	Peak pressure in FLACS (kPa)
1	2 plates @ 5.13m & 9.33m	0.30	45.80	150	170
2	2 plates @ 1.65m & 5.13m	0.50	25.18	405	423
3	No plate	0.00	49.09	12	7
4	1 plate @ 1.65m	0.84	8.10	200	171
5	1 plate @ 1.65m	0.30	8.10	66	65
6	1 plate @ 1.65m	0.16	8.10	50	42
7	1 plate @ 5.13m	0.50	25.18	270	275
8	1 plate @ 5.13m	0.84	25.18	380	400
9	1 plate @ 9.33m	0.50	45.80	90	67

3.3 Simulation of additional separation gap scenarios with small gas cloud of 2300×2300×1500 mm^3

Using the validated FLACS model, simulations of vented explosions of tank groups with additional separation gaps of 250mm, 1250mm and 1500mm were carried out. As mentioned in Section 2, the first three peaks of internal pressures were highly dependent on the failure of polyethylene film. In the tests, the failure pressures of 5 films on different sides of the confined region can be different. Such variations of failure pressure are difficult to control in field tests, whereas it can be eliminated by unifying the failure pressures on all PLASTIC relief panels in

© 2018. This manuscript version is made available under the CC-BY-NC-ND 4.0 license http://creativecommons.org/licenses/by-nc-nd/4.0/

521 CFD simulations. All PLASTIC relief panels were assigned zero opening pressures in the
522 following study. Same as the small gas cloud used in experiments, the gap distance effect was
523 investigated under gas cloud with dimension of 2300×2300×1500 mm^3.

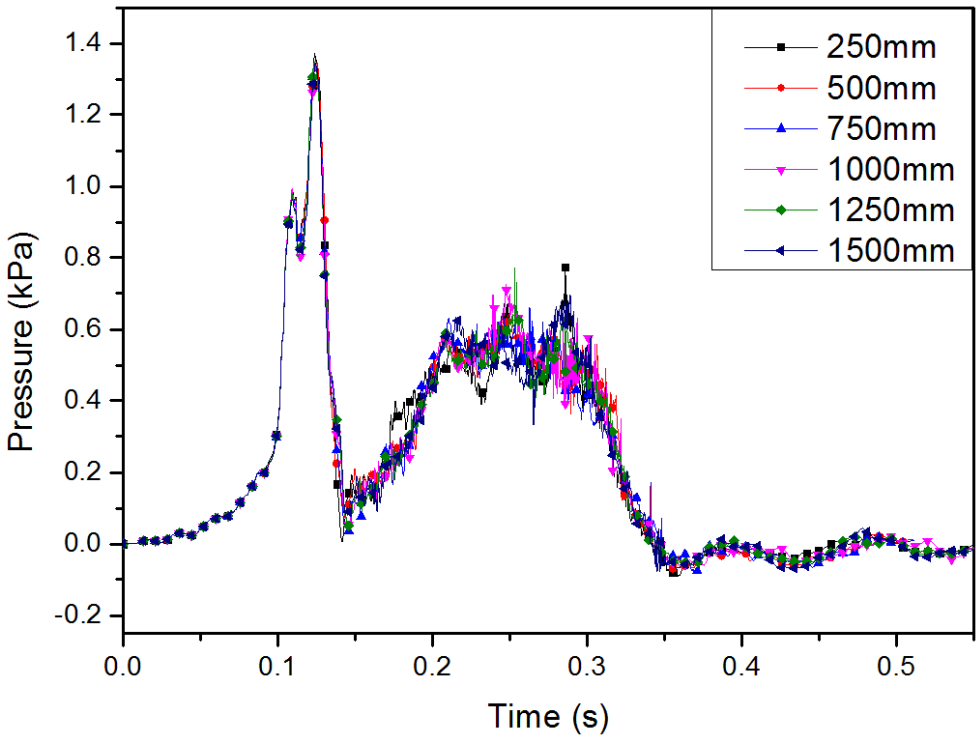

524

525 **(a) Monitor 1**

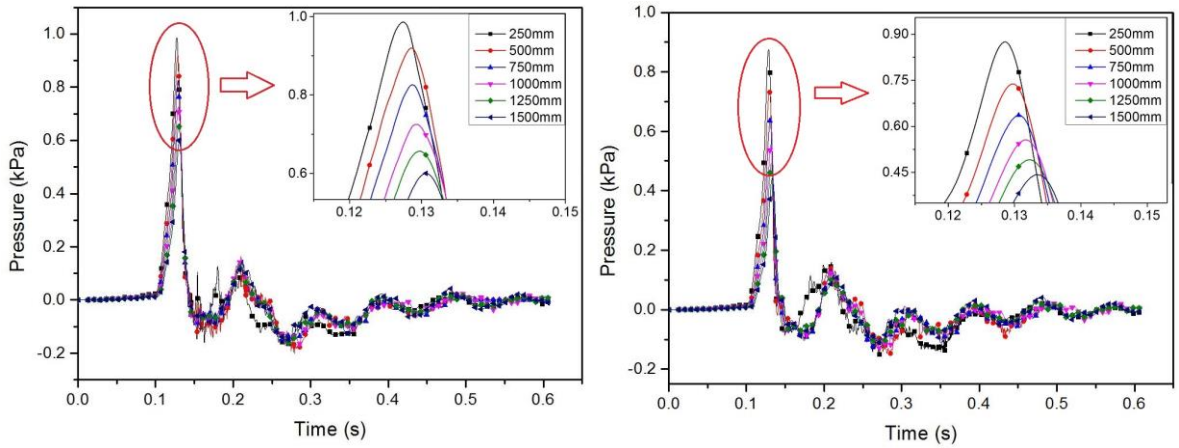

526

527 **(b) Monitor 2** **(c) Monitor 3**

© 2018. This manuscript version is made available under the CC-BY-NC-ND 4.0 license http://creativecommons.org/licenses/by-nc-nd/4.0/

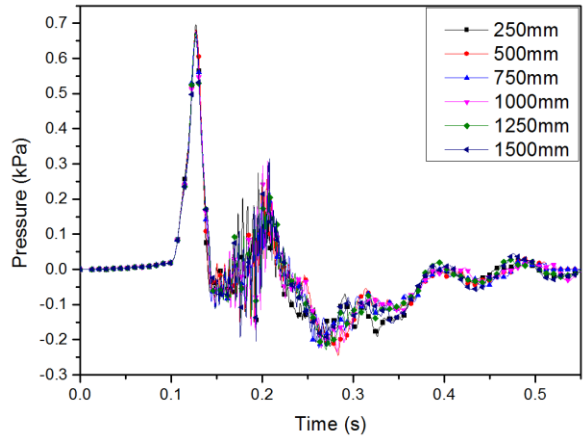

(d) Monitor 4

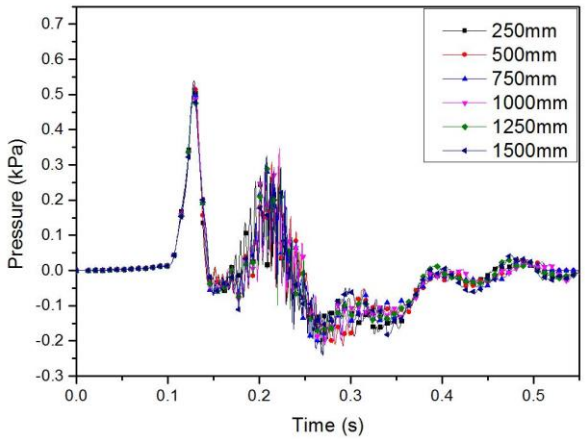

(e) Monitor 5

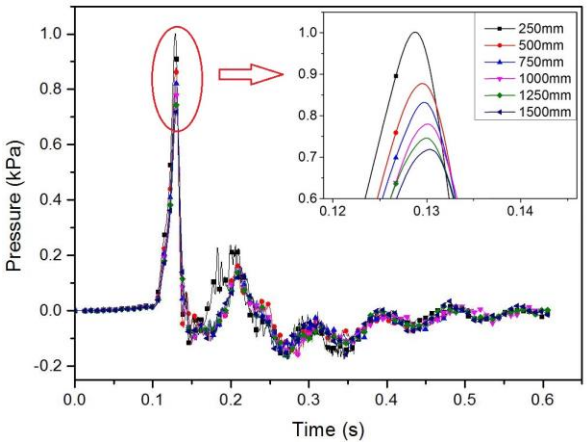

(f) Monitor 6

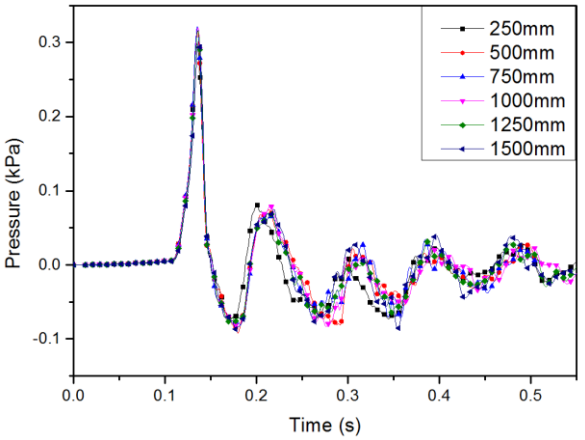

(g) Monitor 7

Fig. 26 Pressure-time data at different locations corresponding to the cases with different separation gaps from gas explosion with a small gas cloud coverage

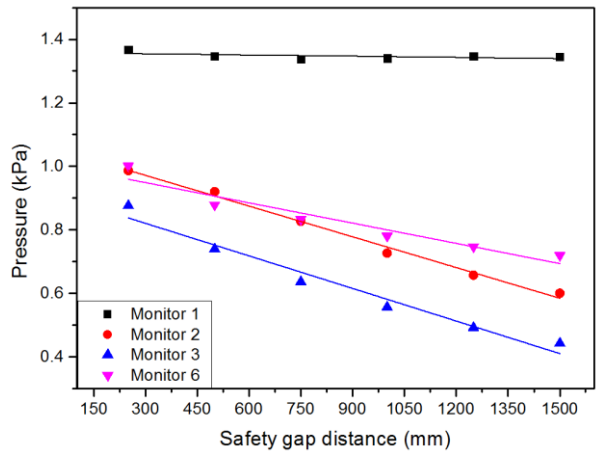

(a) Monitors inside the tank group region

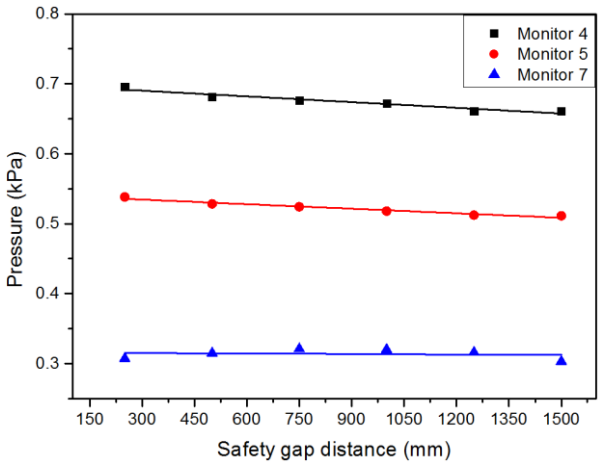

(b) Monitors outside the tank group region

Fig. 27 Maximum pressures recorded at different monitors corresponding to the cases with different separation gaps from gas explosion with a small gas cloud coverage

© 2018. This manuscript version is made available under the CC-BY-NC-ND 4.0 license http://creativecommons.org/licenses/by-nc-nd/4.0/

As seen in Fig. 26 (a), the gap distance has little effect on internal overpressure inside the center tank as all plastic relief panels have zero opening pressures. All pressure peaks were almost identical for all the considered gap distances. On the other hand, obvious pressure weakening with the increase in the separation gap was seen at other locations, i.e., external monitor 2, 3 and 6, which located on the surrounding tank walls. At these three monitors, the pressure development was highly dependent on the flame turbulence between tanks, hence the separation gap played a vital role in mitigating blast pressure.

At the other external monitors (i.e. monitor 4, 5 and 7), the pressure decreasing tendencies are less pronounced than that of monitor 2, 3 and 6, as shown in Fig. 27. It is worth noting that the gas cloud dimensions were 2300×2300×1500 mm^3, the external monitors of No. 4, 5, 7 were not in the gas cloud region. Separation gap between tanks has insignificant effect on the pressure wave propagation outside the cloud. With regard to this statement, justification can be made by relating this study to other researchers' work. So far, limited gas explosion experiments were conducted with multi-obstacle arrays and different pitches/gaps between obstacles (Alekseev et al., 2001; Chan et al., 1983; Harrison and Eyre, 1987; Hjertager et al., 1988; Mercx, 1995; Na'inna et al., 2013). For these studies, it was generally recognized that influence of separation distance between obstacles was an essential parameter in acceleration of turbulence and increase in explosion severity. Although in this study, larger scale tanks were used instead of small obstacles, the effect of separation gap between tanks in Section 2 was shown experimentally to have effect on explosion severity for monitors within the gas cloud, which agreed with the observations in the aforementioned references. Regarding the separation gap effect on external pressure outside of the gas cloud, a CFD simulation (Ma et al., 2014) based on RIGOS experiments (Van den Berg and Mos, 2005) showed that significantly small overpressures were recorded outside of the cloud during explosion. In other words, the turbulence development contributes little to overpressure built-up in the open space without

© 2018. This manuscript version is made available under the CC-BY-NC-ND 4.0 license http://creativecommons.org/licenses/by-nc-nd/4.0/

gas resource. The findings of separation gap effect on explosion pressures in and around the area of a tank group in this study can be used as a general guidance in safety design for medium-scale tanks.

Another noteworthy feature of the pressure-time curves is that the second pressure peaks are much smaller than the first pressure peak at all the monitoring locations, and negative pressures are negligible. The main reason is that the flame acceleration and its time outside the center tank are rather limited due to the small gas cloud volume, therefore, the turbulence induced pressures are relatively small. Higher second pressure peak with longer combustion duration is expected to be seen if the gas cloud volume increased.

3.4 Simulations of explosions of tank group with additional separation gap distances with large gas cloud of 7000×7000×1500 mm^3

To investigate the significance of gas cloud volume on explosion pressures, the gas cloud coverage was increased to 7000×7000×1500 mm^3, as seen in Fig. 28. All other setups were kept the same as those in Section 3.3.

© 2018. This manuscript version is made available under the CC-BY-NC-ND 4.0 license http://creativecommons.org/licenses/by-nc-nd/4.0/

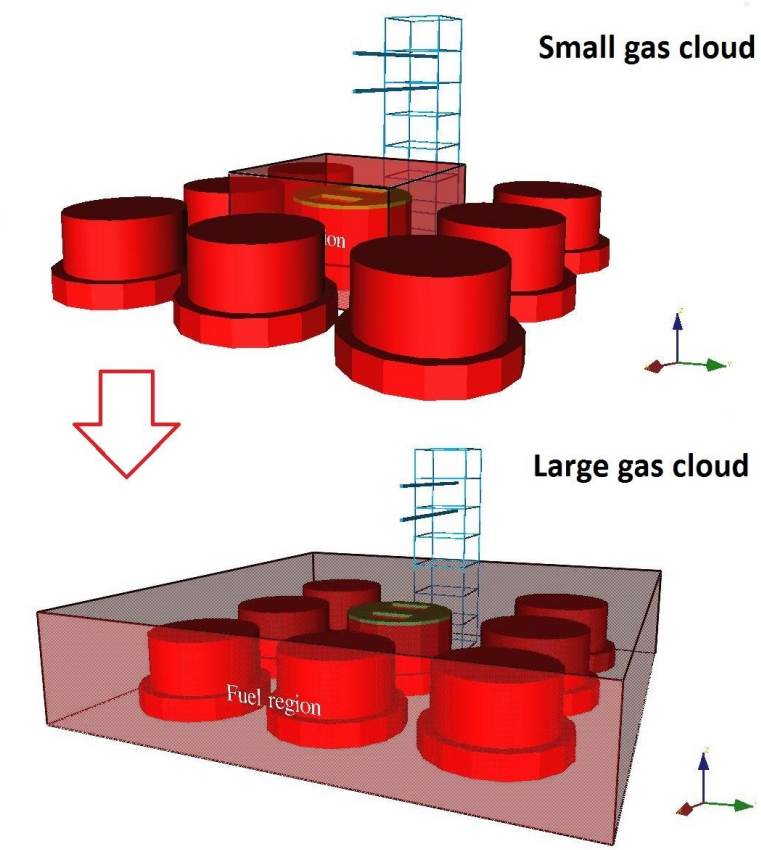

Fig. 28 Gas cloud coverage for the tank group

Pressure-time and impulse-time data were extracted from FLACS post-processor and shown in Fig. 29 and Fig. 30. Compared to the smaller gas cloud coverage in Section 3.3, the second and negative pressure peaks under larger gas cloud coverage became larger. For example, the second pressure peaks at monitor 5 and monitor 7 were even greater than the first peak when the separation gap distance between tanks was 250mm and 500mm.

Additionally, the duration of the second peak was significantly longer than those of the first peak at all monitoring locations. In other words, the second peak contributes more to the total impulse, as seen in Fig. 30. To further investigate the influences of large gas cloud coverage on the pressure time histories, discussions were made with respect to the first peak, the second peak and the negative peak.

© 2018. This manuscript version is made available under the CC-BY-NC-ND 4.0 license http://creativecommons.org/licenses/by-nc-nd/4.0/

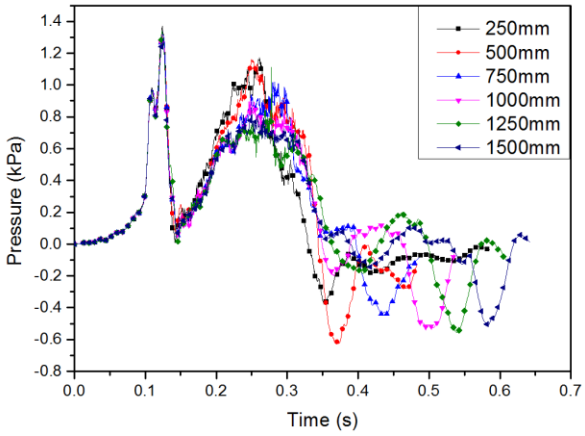

592

593 **(a) Monitor 1**

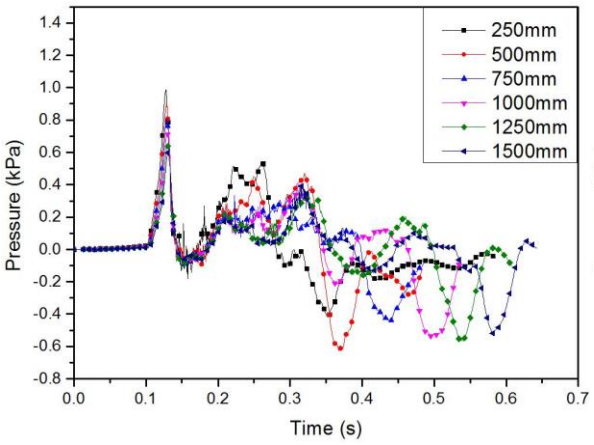

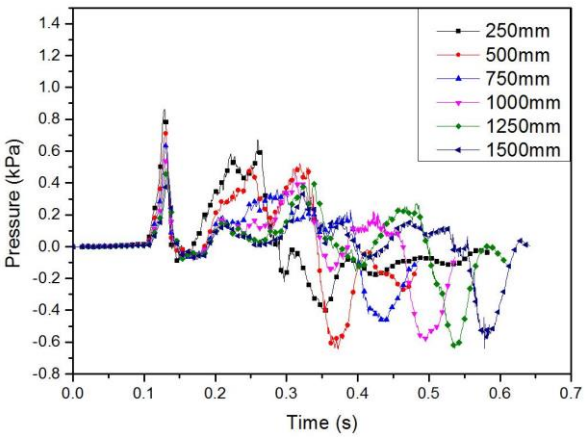

594

595 **(b) Monitor 2** **(c) Monitor 3**

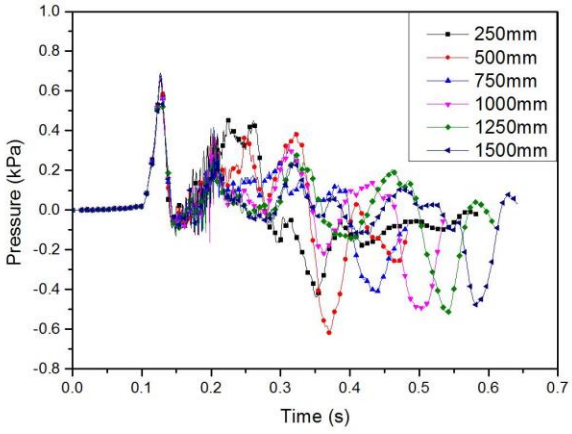

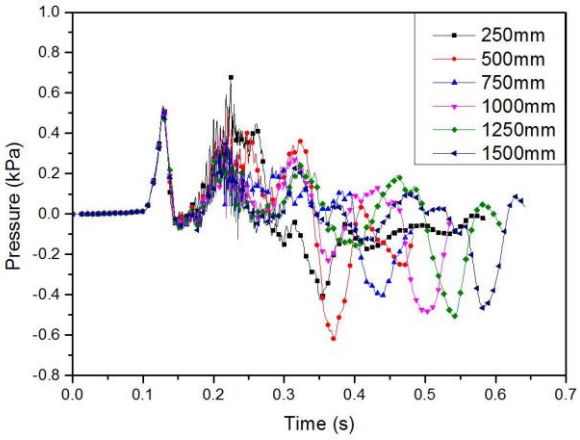

596

597 **(d) Monitor 4** **(e) Monitor 5**

© 2018. This manuscript version is made available under the CC-BY-NC-ND 4.0 license http://creativecommons.org/licenses/by-nc-nd/4.0/

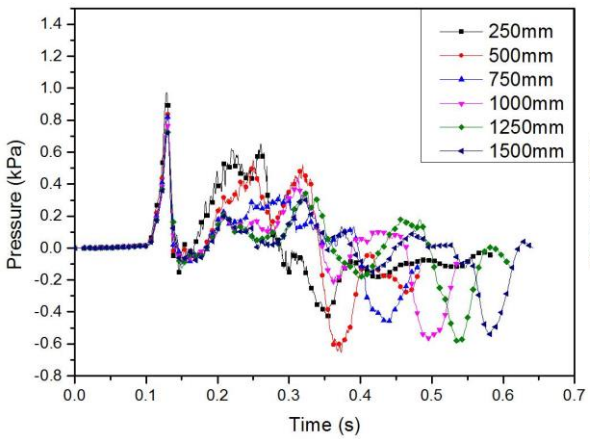

598

599 **(f) Monitor 6**

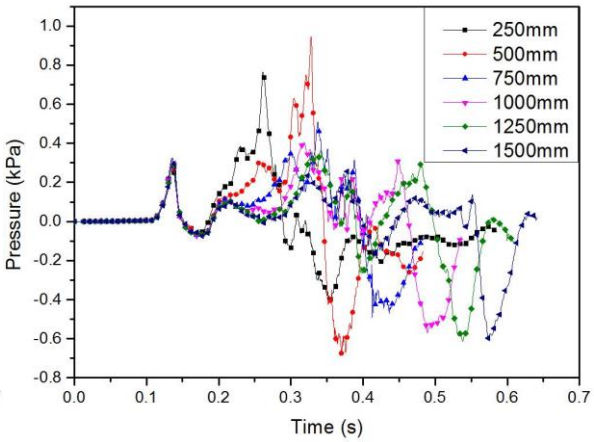

(g) Monitor 7

600 **Fig. 29 Pressure-time histories at different locations with respect to different separation**
601 **gaps from gas explosion under a large gas cloud coverage**

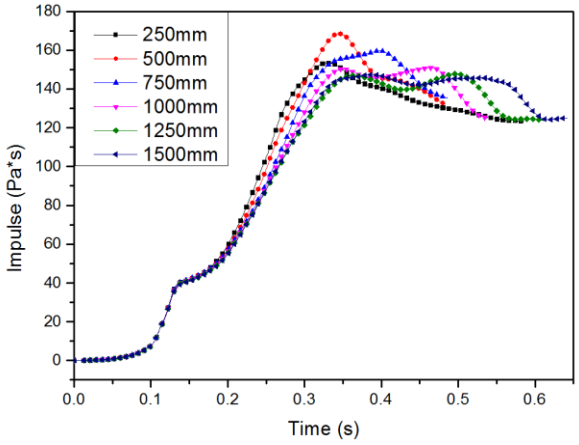

602

603 **(a) Monitor 1**

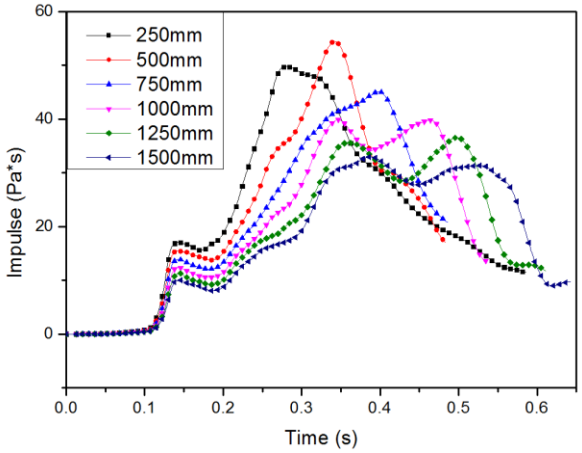

604

605 **(b) Monitor 2**

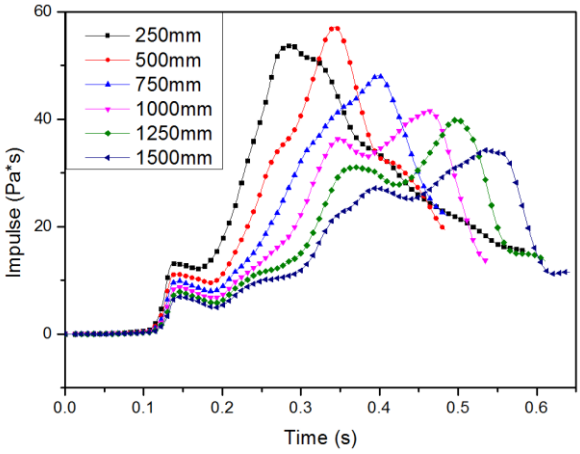

(c) Monitor 3

© 2018. This manuscript version is made available under the CC-BY-NC-ND 4.0 license http://creativecommons.org/licenses/by-nc-nd/4.0/

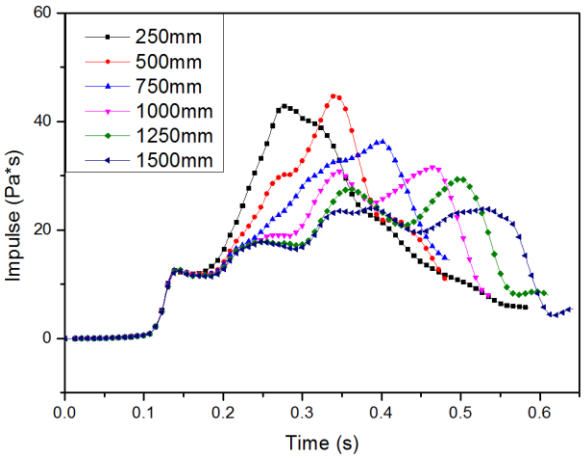

606

607 **(d) Monitor 4**

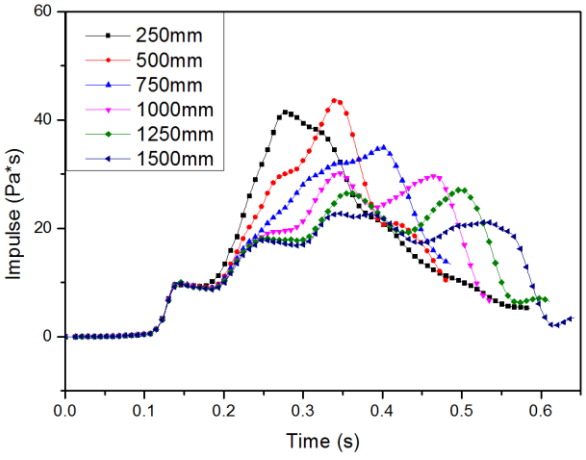

(e) Monitor 5

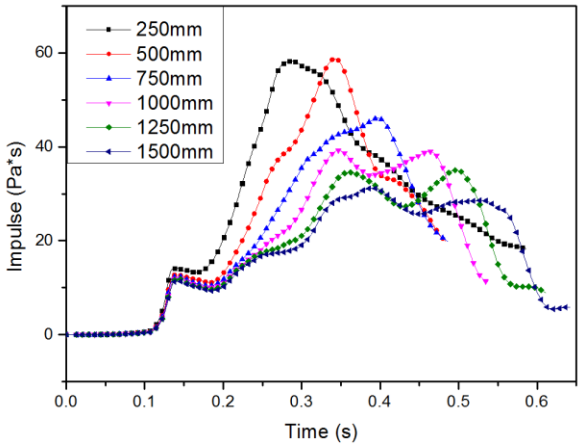

608

609 **(f) Monitor 6**

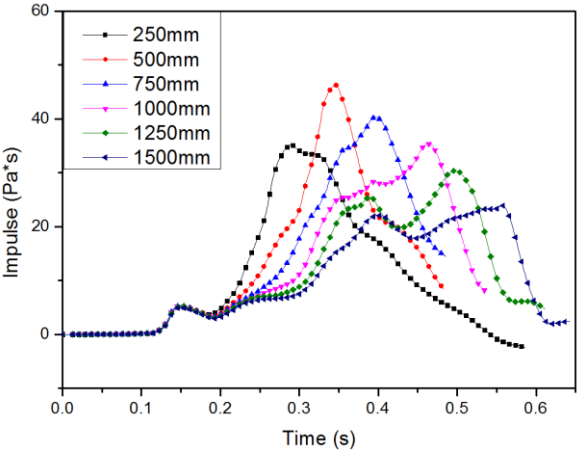

(g) Monitor 7

610 **Fig. 30 Impulse-time data at different locations with respect to different separation gaps from**
611 **gas explosion under a large gas cloud coverage**

612

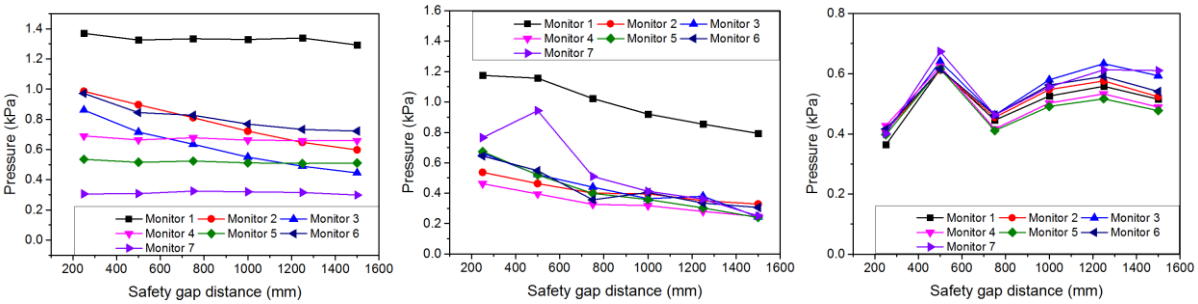

613

614 **(a) First peak** **(b) Second peak** **(c) Negative peak**

615 **Fig. 31 Peak pressure corresponding to different separation gap distances**

© 2018. This manuscript version is made available under the CC-BY-NC-ND 4.0 license http://creativecommons.org/licenses/by-nc-nd/4.0/

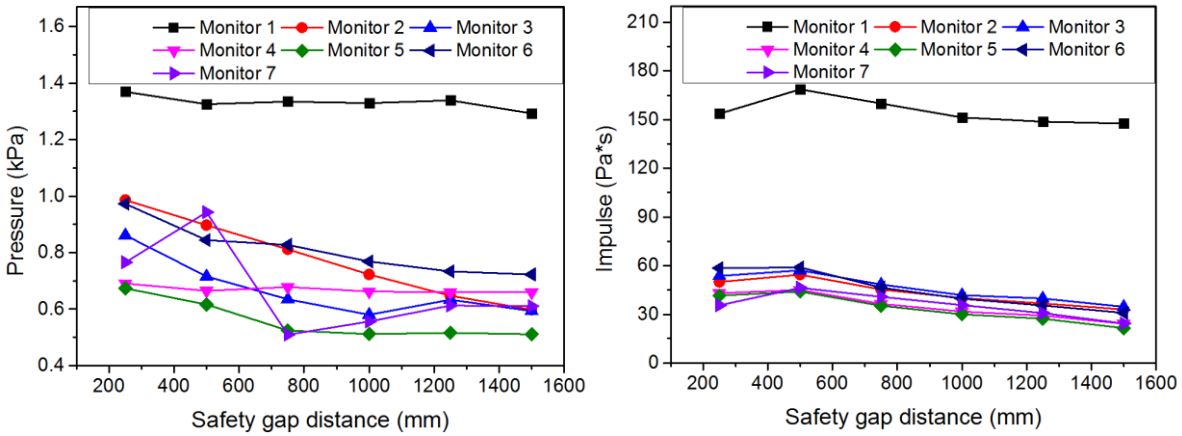

(a) Maximum pressure-gap distance **(b) Impulse-gap distance**

Fig. 32 Maximum pressure-gap distance and impulse-gap distance relations

As seen in Fig. 31(a), the influence of separation gap on first pressure peak under large cloud coverage was similar to that under small cloud coverage shown in Fig. 27, and the apparent decrease of the second peak pressure with separation distance were observed at all locations, except at monitor 7 when the separation distance was 500 mm (in Fig. 31(b)). In general the largest values of the first and the second peak occurred when the separation distance was 250mm. However, the maximum negative pressures were observed when the separation gap was 500 mm among all the considered cases, and the negative peak pressure values did not show a monotonic decreasing trend with the increase of the separation gap. The negative pressures in Fig. 31(c) were reversal pressure peaks (below 0 kPa) obtained from Fig. 29. However, the magnitudes of negative peaks were smaller than the first and second peaks, which means the first peaks and second peaks were more dominant in combustion. Fig. 32 shows the maximum pressure peaks from the three groups and the impulse with respect to the separation gap distance. Compared to the results with small gas cloud shown in Section 3.3, when the gas cloud coverage was sufficiently large that all tanks were covered, all external monitors recorded the pressure peak decreasing with increasing separation gap distance. Among all the cases considered, 250mm gap resulted in the highest pressure peaks but the 500mm separation gap gave the largest impulse.

© 2018. This manuscript version is made available under the CC-BY-NC-ND 4.0 license http://creativecommons.org/licenses/by-nc-nd/4.0/

4 Conclusion and discussion

In this paper, experiments were conducted to investigate the vented gas explosion with three different separation/safety gaps. Different pressure peaks at different combustion time were discussed. The observed internal pressures indicated that the first three peaks before Taylor instabilities were directly proportional to the failure pressure of relief panel. Pressure mitigation due to separation gap was only observed in the fourth peak of internal sensors and other pressure peaks at external sensors located between the tanks.

The CFD simulation was conducted to investigate more vented tank group explosions with different separation gaps. The calibration of CFD simulation results is satisfactory. Based on the same scale testing setup, different cloud coverage scenarios were studied.

For small gas cloud coverage, it is concluded that separation distance has little mitigation effect on internal pressure. Additionally, the secondary pressure peaks and negative pressure peaks, which were much smaller than first pressure peaks, were negligible for all monitors. Separation distance played an essential role in pressure mitigation only for monitors within the gas cloud coverage.

For large gas cloud coverage, three distinct pressure peaks were obtained in this study. Generally, separation gap has little impact on the first internal pressure peak and first external pressure peak in venting direction. While obvious pressure mitigation phenomenon due to separation gap was seen for both of internal and external pressures at the second peaks. The negative pressure peaks were still the least dominant peaks for monitors within gas coverage.

In terms of the maximum pressure, the smallest separation gap of 250mm in this study is deemed to be the most unsafe case regardless of the gas cloud coverage size. However, unlike the logical thinking that the smaller separation gap leads the higher impulse, the 500mm

© 2018. This manuscript version is made available under the CC-BY-NC-ND 4.0 license http://creativecommons.org/licenses/by-nc-nd/4.0/

separation gap instead of 250mm separation gap in the large gas cloud scenario resulted in the highest impulse.

As a practical guidance, it is suggested in this paper that determination of the safe separation distance is dependent on the external pressure and impulse acting on the tank walls. Under the gas cloud coverage, a near-linear correlation between the maximum external pressure on adjacent tank wall and separation gap is expected. Therefore, pressure-wise, the safest separation distance between tanks should be as far as possible. However, in practice, the allowed design distance between gas storage tanks is normally limited. Within a certain distance, the 500mm separation gap case surprisingly has higher impulse than that in the 250mm separation gap case as shown in this study. Therefore, in order to determine the safe distance, detailed CFD simulation is recommended if the allowed distance is limited and close to the tank diameter. Compared to the current regulations which are mainly based on the content flammability, thermal radiation and financial risk analysis, this study provides more insights on the consequences of vented gas explosion, such as the explosion overpressure and impulse applied on adjacent structures.

Acknowledgement

The authors acknowledge partial financial supports from Australian Research Council project (No. LP130100919) and China National 973 project (No. 2015CB058003) for carrying out this research.

© 2018. This manuscript version is made available under the CC-BY-NC-ND 4.0 license http://creativecommons.org/licenses/by-nc-nd/4.0/

References

Alekseev, V.I., Kuznetsov, M.S., Yankin, Y.G., Dorofeev, S.B., 2001. Experimental study of flame acceleration and the deflagration-to-detonation transition under conditions of transverse venting. Journal of Loss Prevention in the Process Industries 14, 591-596.

API-650, 2007. Welded Steel Tanks for Oil Strorage. American Petroleum Institute, 11th Edition.

Arntzen, B.J., 1998. Modelling of turbulence and combustion for simulation of gas explosions in complex geometries, Science and technology division of applied mechanics. The Norwegian University Norway.

Bauwens, C.R., Chaffee, J., Dorofeev, S., 2010. Effect of Ignition Location, Vent Size, and Obstacles on Vented Explosion Overpressures in Propane-Air Mixtures. Combustion Science and Technology 182, 1915-1932.

Bauwens, C.R., Chaffee, J., Dorofeev, S.B., 2011. Vented explosion overpressures from combustion of hydrogen and hydrocarbon mixtures. International Journal of Hydrogen Energy 36, 2329-2336.

Bleyer, A., Taveau, J., Djebaili-Chaumeix, N., Paillard, C.E., Bentaib, A., 2012. Comparison between FLACS explosion simulations and experiments conducted in a PWR Steam Generator casemate scale down with hydrogen gradients. Nuclear Engineering and Design 245, 189-196.

Chan, C., Moen, I.O., Lee, J.H.S., 1983. Influence of Confinement on Flame Acceleration Due to Repeated Obstacles. Combustion and Flame 49, 27-39.

Cooper, M.G., Fairweather, M., Tite, J.P., 1986. On the Mechanisms of Pressure Generation in Vented Explosions. Combustion and Flame 65, 1-14.

Diaz-Ovalle, C., Vazquez-Roman, R., Mannan, M.S., 2010. An approach to solve the facility layout problem based on the worst-case scenario. Journal of Loss Prevention in the Process Industries 23, 385-392.

EN-1473, 2016. EN, BS. Installation and equipment for liquefied natural gas—Design of onshore installations.

Ferrara, G., Di Benedetto, A., Salzano, E., Russo, G., 2006. CFD analysis of gas explosions vented through relief pipes. Journal of Hazardous Materials 137, 654-665.

Gexcon, 2015. FLACS v10.4 User's Manual, Norway.

Harrison, A.J., Eyre, J.A., 1987. The Effect of Obstacle Arrays on the Combustion of Large Premixed Gas Air Clouds. Combustion Science and Technology 52, 121-137.

Hjertager, B.H., 1984. Computer-Simulation of Turbulent Reactive Gas-Dynamics. Modeling Identification and Control 5, 211-236.

Hjertager, B.H., 1993. Computer Modeling of Turbulent Gas-Explosions in Complex 2d and 3d Geometries. Journal of Hazardous Materials 34, 173-197.

Hjertager, B.H., Fuhre, K., Bjorkhaug, M., 1988. Concentration Effects on Flame Acceleration by Obstacles in Large-Scale Methane Air and Propane Air Vented Explosions. Combustion Science and Technology 62, 239-256.

Jung, S.H., Ng, D., Diaz-Ovalle, C., Vazquez-Roman, R., Mannan, M.S., 2011. New Approach To Optimizing the Facility Siting and Layout for Fire and Explosion Scenarios. Industrial & Engineering Chemistry Research 50, 3928-3937.

Li, J.D., Hao, H., 2017. Internal and external pressure prediction of vented gas explosion in large rooms by using analytical and CFD methods. Journal of Loss Prevention in the Process Industries 49, 367-381.

Li, J.D., Hernandez, F., Hao, H., Fang, Q., Xiang, H.B., Li, Z., Zhang, X., Chen, L., 2017. Vented Methane-air Explosion Overpressure Calculation—A simplified approach based on CFD. Process Safety and Environmental Protection 109, 489-508.

© 2018. This manuscript version is made available under the CC-BY-NC-ND 4.0 license http://creativecommons.org/licenses/by-nc-nd/4.0/

Li, J.D., Ma, G.W., Hao, H., Huang, Y.M., 2016. Gas explosion analysis of safety gap effect on the innovating FLNG vessel with a cylindrical platform. Journal of Loss Prevention in the Process Industries 44, 263-274.
Ma, G.W., Li, J.D., Abdel-Jawad, M., 2014. Accuracy improvement in evaluation of gas explosion overpressures in congestions with safety gaps. Journal of Loss Prevention in the Process Industries 32, 358-366.
Mercx, W.P.M., 1995. Modelling and experimental research into gas explosions. Loss Prevention and Safety Promotion in the Process Industries, Vols 1 and 2, A333-A347.
Moen, I.O., Lee, J.H.S., Hjertager, B.H., Fuhre, K., Eckhoff, R.K., 1982. Pressure Development Due to Turbulent Flame Propagation in Large-Scale Methane-Air Explosions. Combustion and Flame 47, 31-52.
Na'inna, A.M., Phylaktou, H.N., Andrews, G.E., 2013. The acceleration of flames in tube explosions with two obstacles as a function of the obstacle separation distance. Journal of Loss Prevention in the Process Industries 26, 1597-1603.
NFPA-59A, 2016. National Fire Protection Association. Standard for the Production, Storage, and Handling of Liquefied Natural Gas (LNG).
Patsiatzis, D.I., Knight, G., Papageorgiou, L.G., 2004. An MILP approach to safe process plant layout. Chemical Engineering Research & Design 82, 579-586.
Pedersen, H.H., Middha, P., 2012. Modelling of Vented Gas Explosions in the CFD tool FLACS. Cisap5: International Conference on Safety & Environment in Process & Power Industry, Pt 1 26, 357-362.
Raj, P.K., Lemoff, T., 2009. Risk analysis based LNG facility siting standard in NFPA 59A. Journal of Loss Prevention in the Process Industries 22, 820-829.
Santos, F.D., Landesmann, A., 2014. Thermal performance-based analysis of minimum safe distances between fuel storage tanks exposed to fire. Fire Safety Journal 69, 57-68.
Tamanini, F., Chaffee, J.L., 1992. Turbulent vented gas explosions with and without acoustically-induced instabilities, Symposium (International) on Combustion. Elsevier, pp. 1845-1851.
Taylor, D.W., 2007. The role of consequence modeling in LNG facility siting. Journal of Hazardous Materials 142, 776-785.
Van den Berg, A., Mos, A., 2005. Research to improve guidance on separation distance for the multi-energy method (RIGOS). HSE.
Van Wingerden, C., Zeeuwen, J., 1983. On the role of acoustically driven flame instabilities in vented gas explosions and their elimination. Combustion and Flame 51, 109-111.
Vyazmina, E., Jallais, S., 2016. Validation and recommendations for FLACS CFD and engineering approaches to model hydrogen vented explosions: Effects of concentration, obstruction vent area and ignition position. International Journal of Hydrogen Energy 41, 15101-15109.
Zhang, M.G., Dou, Z., Liu, L.F., Jiang, J.C., Mebarki, A., Ni, L., 2017. Study of optimal layout based on integrated probabilistic framework (IPF): Case of a crude oil tank farm. Journal of Loss Prevention in the Process Industries 48, 305-311.